

Current Switching of Valley Polarization in Twisted Bilayer Graphene

Xuzhe Ying,^{1,2,3} Mengxing Ye,³ and Leon Balents³

¹*Department of Physics and Astronomy, University of Waterloo, Waterloo, Ontario, N2L 3G1, Canada*

²*School of Physics and Astronomy, University of Minnesota, Minneapolis, MN 55455, USA*

³*Kavli Institute for Theoretical Physics, University of California, Santa Barbara, CA 93106, USA*

(Dated: January 21, 2022)

Twisted bilayer graphene (TBG) aligned with hexagonal boron nitride (h-BN) substrate can exhibit an anomalous Hall effect at $3/4$ filling due to the spontaneous valley polarization in valley resolved moiré bands with opposite Chern number^{1,2}. It was observed that a small DC current is able to switch the valley polarization and reverse the sign of the Hall conductance^{1,2}. Here, we discuss the mechanism of the current switching of valley polarization near the transition temperature, where bulk dissipative transport dominates. We show that for a sample with rotational symmetry breaking, a DC current may generate an electron density difference between the two valleys (valley density difference). The current induced valley density difference in turn induces a first order transition in the valley polarization. We emphasize that the inter-valley scattering plays a central role since it is the channel for exchanging electrons between the two valleys. We further estimate the valley density difference in the TBG/h-BN system with a microscopic model, and find a significant enhancement of the effect in the magic angle regime.

I. INTRODUCTION

Spontaneous ferromagnetism in a purely itinerant electron gas without local moments is an old theoretical idea first imagined by Stoner in the 1930s³. Realizations of this ideal have not been easy to find. The clearest and best studied example is probably quantum Hall ferromagnetism^{4,5}, where the Stoner instability is enabled by the flatness of Landau levels induced by an orbital magnetic field. Quantum Hall ferromagnetism is, however, not ultimately true ferromagnetism insofar as time-reversal symmetry is from the outset strongly and explicitly broken by a large applied magnetic field. Recently, purely itinerant ferromagnetism has been observed in zero magnetic field in twisted bilayer graphene (TBG), adding to the host of exotic phenomena in this system when twisted near the “magic angle” at which the moiré bands becomes exceptionally flat^{1,2,6-30}. The most dramatic signatures of itinerant ferromagnetism occur in TBG samples aligned to an hexagonal-Boron Nitride (h-BN) substrate at $3/4$ filling^{1,2}. Here the ferromagnetism observed below the Curie temperature of $5 - 8K$ is observed via an anomalous Hall effect (AHE) – a zero field hysteretic Hall resistivity – that evolves into a quantized value of $\rho_{xy} = h/e^2$ at low temperature: a quantum anomalous Hall effect (QAHE). The existence of the QAHE, which has been discussed extensively theoretically^{10,31,32}, is related to two aspects of TBG. First, graphene itself has incipient valley Chern number associated to its Dirac points, which is created even in a single layer by an infinitesimal perturbation breaking inversion or C_2 rotation or time-reversal \mathcal{T} symmetries. In TBG this extends to bands formed from both layers, and with h-BN to break the $C_2\mathcal{T}$, and the 4 active moiré bands acquire unit Chern number with sign that is opposite for conduction and valence bands and opposite for each valley. The second necessary aspect for (Q)AHE in TBG is symmetry breaking. An AHE then is observed when the difference of occupation of the two

valleys – the valley polarization Φ_v – becomes non-zero. This signifies spontaneous breaking of \mathcal{T} symmetry and defines ferromagnetism. The presence of QAHE implies that *at low temperature* both spin and valley symmetries are broken, and both are fully polarized. Note that for the AHE at temperatures close to the Curie point, the valley polarization Φ_v is the order parameter, and spin symmetry breaking is not essential. The sign of the Hall conductivity is determined by the valley polarization, so that tuning the latter controls the former.

Interestingly, in experiment, the sign of the Hall conductance can be controlled by either an external magnetic field or a bias electric field/current^{1,2}. Similar hysteresis curves were observed on sweeping either the magnetic field or the DC current, indicating an apparent first order transition in the valley polarization, similar to the way in which the magnetic field affects the magnetization in the Ising model.

The sensitive magnetic field control of the valley polarization and thus the Hall conductance has been well explained by linear free energy dependence associated to the giant orbital magnetic moment of the moiré Bloch electrons^{1,2,33,34}, which is closely related to the large Berry curvature of the valley Chern bands. The mechanism for current switching of the Hall conductance remains less clear. Several proposals have been made for this mechanism at low temperature^{1,35,36}. Here, we focus on higher temperatures near but below the Curie point. In experiment, the sign of the Hall conductance remains sensitive to the DC current in this regime, where indeed experiments are significantly easier and more reproducible, due to weakness of hysteresis. At these temperatures, the bulk is dissipative $\sigma_{xx} \neq 0$ and σ_{xy} is not quantized, and indeed the Hall angle $\theta_H \sim \sigma_{xy}/\sigma_{xx} \ll 1$ is small.

In this highly conducting situation, it may be tempting to make analogies to current switching of common metallic ferromagnets, where it is usually ascribed to “spin torque”. However, some important differences are

evident. First, in TBG, the magnetization itself is primarily orbital, and indeed we do not expect significant spin polarization near the Curie point. Second, a related point is that normal ferromagnets have an approximate spin-rotation symmetry (arising from weak spin-orbit coupling) and the ferromagnetism is described by a vector order parameter with weak anisotropies; in contrast, in TBG the valley polarization is Ising-like and not a vector. The Ising symmetry that changes the sign of the valley polarization is just \mathcal{T} . Finally, in clean TBG there is to an excellent approximation a valley conservation symmetry. This is not the symmetry spontaneously broken by the AHE, but rather it implies that the valley polarization order parameter is approximately *conserved*.

In this article, we report a mechanism that takes these features into account and leads to the control of valley polarization by a DC current. As a consequence of the quasi-conservation of the order parameter, in this mechanism, inter-valley scattering plays a central role. We first study the dynamics of the valley polarization order parameter (VPOP) near the Curie temperature T_c by obtaining its equation of motion (EoM). The EoM shows that any mechanism which can generate an electron density difference between the two valleys in the non-interacting model can induce a first order transition of the VPOP. By solving the semiclassical Boltzmann equation, we show that the valley density difference can be generated by a DC current with inter-valley scattering that breaks the rotational symmetry to \mathcal{C}_{1z} . We find that the valley density difference is proportional to the current density, the inverse of the Fermi velocity and the strength of the rotational symmetry breaking. We make a specific estimate for the magnitude of the effect for TBG aligned with h-BN (denoted as TBG/h-BN system hereafter), and demonstrate two sources of enhancement in comparison with the single layer graphene. First, we show an enhancement of the effective strain from ϵ in single layer graphene to ϵ/θ_w in TBG with twist angle θ_w . Second, near the magic twist angle, the Fermi velocity is significantly reduced from 10^6 m/s to around $10^4 - 10^5$ m/s. Combining the two effects, the enhancement of the current induced valley density difference is on the order of 10^3 . Thus, the valley polarization is very sensitive to the applied DC current.

The rest of the paper is organized as follows. In Sec. II, we introduce the model, discuss the dynamics and steady state solution of the valley polarization order parameter, and demonstrate how it can be controlled by a DC current qualitatively. To obtain this relation quantitatively, in Sec. III, we present the Boltzmann equation and estimate the inter-valley scattering rate for the TBG/h-BN system. The technical details are postponed to the Appendix. App. A derives the dynamics of VPOP within the Keldysh formalism. App. B presents the details of the modeling of the TBG/h-BN system.

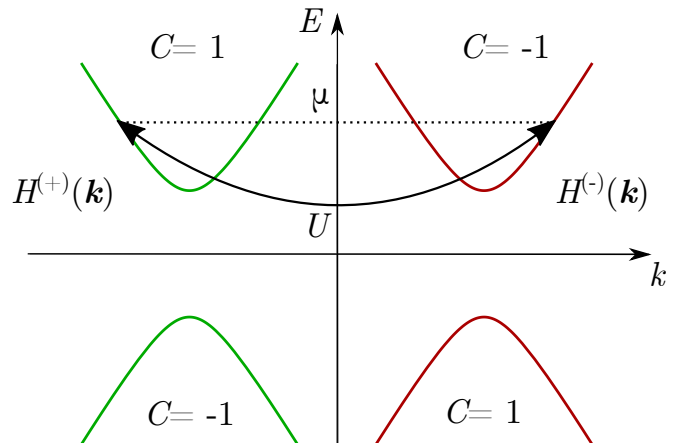


FIG. 1. Schematic of model with two valleys, with a Stoner-type interaction. The two valleys are time reversal related, so that they carry opposite Chern numbers.

II. VALLEY POLARIZATION

In this section, we discuss the dynamics of the valley polarization order parameter. We employ the nonequilibrium Keldysh approach³⁷, and obtain the equation of motion (EoM) for the valley polarization order parameter (VPOP) due to the interplay between the interaction and the external current. This construction demonstrates the relation between the current (or magnetic field) induced polarization of non-interacting electrons, Δn_0 , and the true polarization (the VPOP) Φ_v , including interactions.

II.1. The Model

In this article, we consider a model with 2 copies of Chern insulators labeled as $s = \pm$, Fig. 1, with the following free fermion Hamiltonian:

$$H_0 = \sum_{i=\pm} \psi_{\mathbf{k}}^{(s)\dagger} H^{(s)}(\mathbf{k}) \psi_{\mathbf{k}}^{(s)}. \quad (1)$$

The two copies of Chern insulators are further assumed to be related by the time reversal symmetry \mathcal{T} , such that $\mathcal{T}H^{(\pm)}(\mathbf{k})\mathcal{T}^{-1} = H^{(\mp)}(-\mathbf{k})$. With the restriction from the time reversal symmetry, the two conduction bands (as well as the valence bands) carry opposite Chern number, Fig. 1. This model may be considered as a low energy effective model for the TBG/h-BN system¹³, when only the 2 active moiré bands (in sublattice space) in each valley is included, and each copy of a Chern insulator corresponds to a valley. Thus, the two copies of Chern insulators are referred to as two valleys in the rest of the article.

To model the interaction induced valley polarization, we restrict the interaction to the inter-valley density-density channel only:

$$H_{\text{int}} = U \int d\mathbf{x} n^{(+)}(\mathbf{x}) n^{(-)}(\mathbf{x}), \quad (2)$$

where U is the interaction strength that we approximate as a constant, and $n^{(\pm)}$ is the electron density of the \pm valleys. This is a caricature of the inter-valley component of the Coulomb interaction. We expect that the precise form of the interaction is not important, so long as the symmetries of the problem (time-reversal and valley conservation) are respected, as we will be primarily interested in low energy quantities in the vicinity of the Curie point. At strong interaction $U > U_c$, the valley polarization develops spontaneously at low temperature. The critical interaction U_c can be estimated to be the inverse of the density of states at Fermi level according to the Stoner criteria, i.e. $U_c \sim \nu^{-138}$.

Note that the spin degrees of freedom are ignored in our study. As discussed in the Introduction, the AHE requires only valley and not spin polarization. Furthermore, in the vicinity of the Curie point, there is unlikely to be substantial spin polarization, since with SU(2) spin symmetry the Mermin-Wagner theorem³⁹ prohibits any $T > 0$ order, and SU(2) spin symmetry is broken extremely weakly by tiny spin-orbit and dipolar effects.

II.2. Steady State Solution of the Valley Polarization Order Parameter

We now obtain the EoM of the VPOP using the non-equilibrium Keldysh approach. Details of the derivations are given in App. A. It is essential to introduce a proper scattering mechanism in order to establish a steady state subject to an electric field. We consider short ranged disorder described by an impurity potential $V^{\text{imp}}(\mathbf{x})$, which induces both intra- and inter-valley scattering [see Eq. (A10)].

Near the transition temperature ($T \sim T_c$), the EoM can be expressed as an expansion in powers of the VPOP Φ_v . It takes the form

$$\alpha_2(\omega, q)\Phi_v + \alpha_4\Phi_v^3 + \Delta n_0 = 0, \quad (3)$$

which should be regarded as somewhat symbolic, with the time and space dependence expressed in the first term in Fourier space, while the second and third terms may be considered approximately local. To the leading order in $|T - T_c|$ and external bias electric field, quadratic terms $\sim \alpha_3 h^2$ can be ignored (they vanish in equilibrium without any symmetry breaking field). In the static limit for the homogeneous order parameter, i.e. $\omega = 0$ and then $\mathbf{q} \rightarrow 0$, this reduces to the standard expression that mimics the 1st order Ising phase transition in an external field, i.e.

$$(r - r_c)\Phi_v - \alpha_4\Phi_v^3 = \Delta n_0, \quad (4)$$

where Δn_0 is the valley density difference that would be induced by the bias electric field in the absence of interactions (and hence is smooth near T_c because the transition is induced by interactions). The quantity $(r - r_c) = -\alpha_2(0, 0) \sim (T/T_c - 1)^{38}$ changes sign across the equilibrium transition. The cubic coefficient

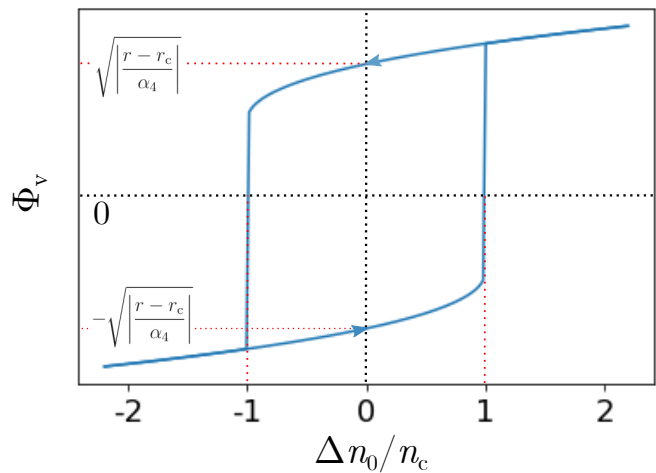


FIG. 2. Hysteresis curve for valley polarization Φ_v upon tuning the valley density difference Δn_0 at $T < T_c$. The coercive valley density difference is $n_c = -2\alpha_4 \left(\frac{r-r_c}{3\alpha_4}\right)^{3/2}$.

$-\alpha_4 \sim |\nu''(\epsilon_F)|U^3$ is positive definite, corresponding to a bounded equilibrium free energy, and ensures the stability of the state across the transition. By construction, the VPOP describes the expectation value of the valley density difference, $\Phi_v = (\langle n^{(+)} \rangle - \langle n^{(-)} \rangle)$ (see App. A). Keep in mind that Δn_0 is valley density difference induced by the external bias field alone without interactions, while the VPOP Φ_v describes the valley density difference with both the external bias field and interactions taken into account.

Without the bias electric field, $\Delta n_0 = 0$, Eq. (4) describes spontaneous \mathbb{Z}_2 symmetry breaking in equilibrium when $T < T_c$ [$(r - r_c) < 0$], with $\Phi_v = \pm \sqrt{|(r-r_c)/\alpha_4|}$. Non-zero Δn_0 explicitly breaks the \mathbb{Z}_2 symmetry, and selects the + or - VPOP, when Δn_0 is positive or negative, respectively. By tuning Δn_0 , one recovers the hysteresis curve, Fig. 2. The coercive valley density difference is given by $n_c = -2\alpha_4 \left(\frac{r-r_c}{3\alpha_4}\right)^{3/2}$.

To address how the external bias electric field controls the valley polarization, we discuss below how Δn_0 depends upon the bias electric field \mathbf{E} , or equivalently the current density \mathbf{j} . Importantly, breaking lattice rotational symmetry is necessary to generate any valley density difference by the current \mathbf{j} . This is because the bias electric field and current, \mathbf{E} and \mathbf{j} , are vectors in 2D. To make a non-zero scalar, Δn_0 , another vector is needed. This means that there is a particular direction in the sample. Thus, the (discrete) rotational symmetry has to be broken.

Moreover, by dimensional analysis, one can easily show that the valley density difference generated by an applied DC current should be given by:

$$\Delta n_0 \simeq \frac{a}{ev_F} j_x + \frac{b}{ev_F} j_y = \frac{1}{ev_F} \mathbf{j} \cdot \boldsymbol{\delta}_\epsilon, \quad (5)$$

which is proportional to the current density in 2D, $\mathbf{j} =$

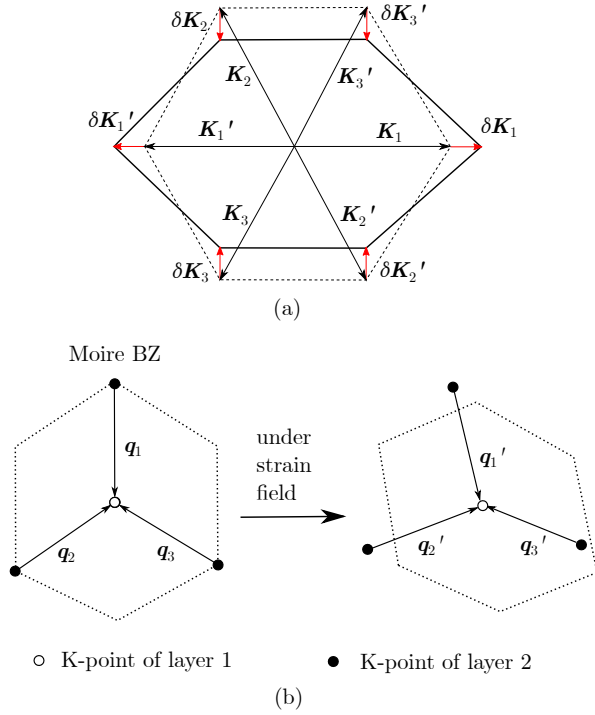


FIG. 3. (a) Brillouin zone (BZ) of single layer graphene with uniaxial strain; (b) moiré Brillouin zone without (left) and with (right) uniaxial strain. The C_3 symmetry of the unstrained moiré BZ is explicitly broken by the strain field.

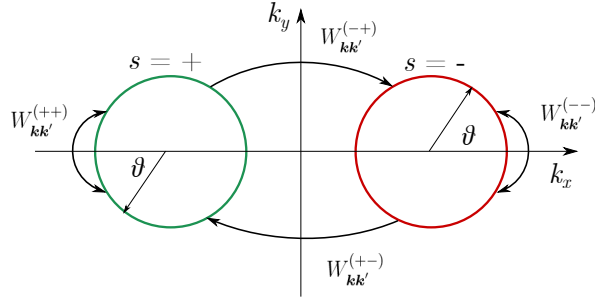


FIG. 4. Impurity scattering between two Fermi pockets.

(j_x, j_y) , and inverse of the Fermi velocity v_F . The dimensionless parameters, $a(b)$ or δ_ϵ , are related to the broken rotational symmetry. They are also highly dependent on the microscopic details of the system, which we do not attempt to address in depth in this article.

Following the general discussion above, one may qualitatively argue that in the TBG/h-NB system, the valley density difference generated by a DC current can be quite

significant for two reasons. First, the small Fermi velocity of the flat bands near the magic angle increases Δn_0 by a factor on the order of $10^2 - 10^3$. Second, the smallness of the moiré Brillouin zone enhances the proportional effect of strain, as follows. Strain results in anisotropy in the electronic spectrum, reflected in a shift of the location of the Dirac point, $\delta\mathbf{K}$, directional dependence of the Dirac velocity, δv_D , etc. For single layer graphene, the anisotropy can be characterized by a small parameter, for example the strain strength, $\epsilon \sim \frac{|\delta\mathbf{K}|}{|\mathbf{K}|}$, $\frac{\delta v_D}{v_D}$, see Fig. 3(a). For strained TBG, as in Fig. 3(b), the shift of the Dirac points should be compared with the size of the moiré BZ. Thus, the broken C_3 symmetry is actually characterized by $\frac{\epsilon}{\theta_w} \sim \frac{|\delta\mathbf{K}|}{q}$, where θ_w , $q = |\mathbf{K}|\theta_w$ are the small twist angle and distance between the adjacent Dirac points of the two graphene layers due to the twist, an enhancement of a factor of $1/\theta_w$ due to moiré physics. These two effects enhance the dimensionless parameters δ_ϵ in Eq. (5), which are thus not necessarily small, and the effect may be quite significant.

III. CURRENT INDUCED VALLEY DENSITY DIFFERENCE

In this section, we employ the semi-classical Boltzmann equation to demonstrate how a DC current may induce a valley density difference Δn_0 for models without rotational symmetry, and estimate the dimensionless coefficient δ_ϵ for TBG aligned with h-BN.

III.1. Toy Model and the Semi-classical Formalism

In this subsection, we demonstrate the effect of inter-valley scattering on the current induced valley density difference Δn_0 by solving the semi-classical Boltzmann equation (SBE). We simplify the Fermi surface at each valley as a circular Fermi pocket as shown in Fig. 4, and will argue later that this simplification doesn't change the result qualitatively. The calculation is carried out in the absence of interactions, i.e. in the paramagnetic phase, so that time reversal symmetry is present, which imposes $\epsilon^s(\mathbf{k}) = \epsilon^{\bar{s}}(-\mathbf{k})$ and $\mathbf{v}^s(\mathbf{k}) = -\mathbf{v}^{\bar{s}}(-\mathbf{k})$, where $s = \pm$ is the valley index with $s \neq \bar{s}$. No other point group symmetries are assumed.

The SBE within the presence of a bias electric field \mathbf{E} is given by^{37,40}:

$$\partial_t f_{\mathbf{k}}^{(s)} + \mathbf{v}_{\mathbf{k}}^{(s)} \cdot \partial_{\mathbf{x}} f_{\mathbf{k}}^{(s)} + e\mathbf{E} \cdot \partial_{\mathbf{k}} f_{\mathbf{k}}^{(s)} = \sum_{s'=\pm} \int d\Gamma' W_{\mathbf{k}\mathbf{k}'}^{(ss')} \left(f_{\mathbf{k}'}^{(s')} - f_{\mathbf{k}}^{(s)} \right) \delta(\epsilon_{\mathbf{k}'}^{(s')} - \epsilon_{\mathbf{k}}^{(s)}) = I_{\text{intra}}^{(s)}[f_{\mathbf{k}}] + I_{\text{inter}}^{(s)}[f_{\mathbf{k}}]. \quad (6)$$

The measure in the collision integral is defined as $d\Gamma' =$

$\frac{d^2 k'}{(2\pi)^2}$. Both the intra-valley scattering, $W_{\mathbf{k}\mathbf{k}'}^{(++)}$ and

$W_{\mathbf{k}\mathbf{k}'}^{(--)}$, as well as the inter-valley ones, $W_{\mathbf{k}\mathbf{k}'}^{(-+)}$ and $W_{\mathbf{k}\mathbf{k}'}^{(+-)}$, are included. TRS requires that $W_{\mathbf{k}\mathbf{k}'}^{(++)} = W_{\mathbf{k}'\mathbf{k}}^{(--)}$ and $W_{\mathbf{k}\mathbf{k}'}^{(-+)} = W_{\mathbf{k}'\mathbf{k}}^{(+-)}$. Here, we assume detailed balance, which follows from the first Born approximation.

$$f_{\mathbf{k}}^{(s)} = f_0 + x_0^{(s)} \frac{\partial f_0}{\partial \epsilon} + \sum_{n=1}^{\infty} x_n^{(s)} \cos n\theta_{\mathbf{k}} \frac{\partial f_0}{\partial \epsilon} + \sum_{n=1}^{\infty} y_n^{(s)} \sin n\theta_{\mathbf{k}} \frac{\partial f_0}{\partial \epsilon}, \quad (7)$$

where f_0 is the equilibrium Fermi distribution function, the angle $\theta_{\mathbf{k}}$ is defined for each valley as shown in Fig. 4. The harmonic coefficients, $x_n^{(s)}$ and $y_n^{(s)}$, are proportional to \mathbf{E} within linear response. The valley density difference is determined by:

$$\begin{aligned} \Delta n_0 &= n^{(+)} - n^{(-)} = \int d\Gamma \left(f_{\mathbf{k}}^{(+)} - f_{\mathbf{k}}^{(-)} \right) \\ &= -\nu \left(x_0^{(+)} - x_0^{(-)} \right), \end{aligned} \quad (8)$$

where ν is the density of states at the Fermi level. Notice that the simplification to the second line of Eq. (8) is a result of the assumed circular Fermi pockets, see Fig. 4.

Before presenting the solution of the Boltzmann equation, we point out the central role of inter-valley scattering. Namely, to obtain non-zero valley density difference, Δn_0 , the inter-valley scattering rate must be treated with care. In particular, a constant inter-valley scattering rate $1/\tau'$ cannot generate a nonzero valley density difference in the static limit. To see this point, one can integrate the SBE, Eq. (6), over the full Brillouin zone, assuming that the inter-valley scattering rate is a constant, W^{inter} . The result is a continuity equation for the valley densities: $\partial_t n^{(\pm)} - \nabla \cdot \mathbf{j}^{(\pm)} = -(n^{(\pm)} - n^{(\mp)})/\tau'$, where the inter-valley scattering time is defined as $\tau'^{-1} = \nu W^{\text{inter}}$. In a spatially uniform and time independent system, the right hand side must vanish, which indicates that the valley density difference always relaxes and vanishes in the static limit, even though we allowed for non-zero (but constant) inter-valley scattering. To avoid this problem, one must account for momentum-dependent inter-valley scattering, which will induce a ‘‘source’’ in the continuity equation.

Following the reasoning above, we consider the inter-valley scattering rate given by:

$$W_{\mathbf{k}\mathbf{k}'}^{(-+)} = W_{\mathbf{k}'\mathbf{k}}^{(+-)} = \frac{1}{\nu\tau'} \left(1 + a_1 \cos \theta_{\mathbf{k}} + b_1 \sin \theta_{\mathbf{k}} + a'_1 \cos \theta_{\mathbf{k}'} + b'_1 \sin \theta_{\mathbf{k}'} \right) \quad (9)$$

which explicitly breaks rotational symmetry. The dimensionless parameters a_1, a'_1 and b_1, b'_1 are determined by the microscopic mechanisms of breaking rotational symmetry.

For demonstration purposes, we make two additional simplifications. First, we assume the intra-valley scatter-

We look for a static solution of the SBE, Eq. (6), within linear response. The distribution function can be conveniently parameterized by harmonic coefficients:

ing is constant,

$$W_{\mathbf{k}\mathbf{k}'}^{(++)} = W_{\mathbf{k}\mathbf{k}'}^{(--)} = \frac{1}{\nu\tau}, \quad (10)$$

where ν and τ are the density of states and the intra-valley scattering time, respectively. Second, the Fermi surfaces are assumed to be circular. Indeed, given the inter-valley scattering rate in Eq. (9), the detailed form of the intra-valley scattering and the Fermi surface geometry are expected to play a secondary role on the generation of valley polarization. They do not affect whether a valley density difference can be generated by external bias or not. They only affect the magnitude of the valley density difference, at a similar level to other microscopic details that are beyond our model calculations.

The solution to Eq. (6) is physically intuitive in the limit that the intra-valley scattering time (τ) is much shorter than the inter-valley one (τ'). To leading order in τ/τ' , the static solution satisfies the SBE with *only* the intra-valley scattering,

$$e\mathbf{E} \cdot \mathbf{v}_{\mathbf{k}}^{(s)} \frac{\partial f_0}{\partial \epsilon} = I_{\text{intra}}^{(s)}[f_{\mathbf{k}}]. \quad (11)$$

The harmonic expansion coefficients of the distribution function are

$$\begin{cases} x_n^{(s)} = 0 & y_n^{(s)} = 0 & \text{if } n \neq 0, 1 \\ x_1^{(s)} = s e E_x v_F \tau & y_1^{(s)} = s e E_y v_F \tau \end{cases}, \quad (12)$$

where τ is the intra-valley scattering time, v_F is the Fermi velocity defined from $\mathbf{v}_{\mathbf{k}_F}^{(s)} = s v_F (\cos \theta_{\mathbf{k}}, \sin \theta_{\mathbf{k}})$. Note that without inter-valley scattering, there is no constraint on $x_0^{(s)}$ from the SBE because the number density of each valley is separately conserved.

Now the static valley density difference can be determined by solving $0 = I_{\text{inter}}^{(s)}[f_{\mathbf{k}}]$:

$$0 = x_0^{(+)} - x_0^{(-)} + \frac{1}{2} \left(a'_1 x_1^{(+)} + b'_1 y_1^{(+)} - a_1 x_1^{(-)} - b_1 y_1^{(-)} \right). \quad (13)$$

This equation dictates a balance between the inter-valley relaxation process (the first two terms) and a ‘‘source’’ (the last term in parentheses) that generates the valley density difference. The ‘‘source’’ originates from the interplay between the nonequilibrium distribution function

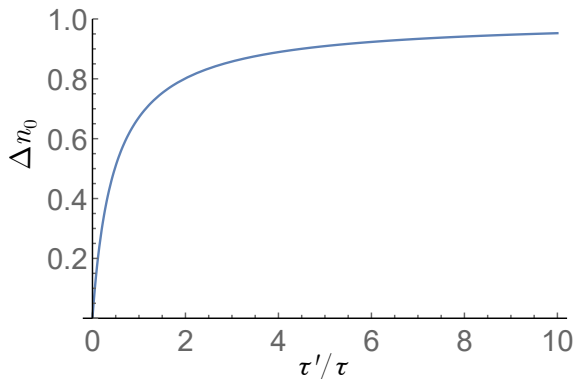


FIG. 5. The valley density difference, Δn_0 , as a function of the ratio of the inter- and intra valley scattering time, τ'/τ . The density is normalized to the value of Eq. (15).

from Eq. (12) and the rotational symmetry breaking of the inter-valley scattering rate, Eq. (9).

Solving Eq. (13), we find that the valley density difference $\Delta n_0 = n^{(+)} - n^{(-)}$ is given by:

$$\Delta n_0 = \frac{\nu v_F \tau}{2} [eE_x (a_1 + a'_1) + eE_y (b_1 + b'_1)], \quad (14)$$

or, equivalently expressed in terms of the current density $\mathbf{j} = \sigma \mathbf{E}$:

$$\Delta n_0 = \frac{1}{2h\nu_F} \frac{h}{e^2} [ej_x (a_1 + a'_1) + ej_y (b_1 + b'_1)]. \quad (15)$$

Notice the bulk longitudinal conductivity σ is related to the intra-valley scattering rate τ through $\sigma = 2\frac{e^2}{h}\nu D$, where $D = \frac{1}{2}v_F^2\tau$ is the two dimensional diffusion constant and the prefactor of 2 accounts for the two valleys.

The simplified model presented in this subsection can be solved exactly. The valley density difference for a general ratio of inter- and intra-valley scattering time, τ'/τ , is shown in Fig. 5. Indeed, when the inter-valley scattering time is much longer than the intra-valley one, the valley density difference saturates to a value given by Eq. (15). On the other hand, Δn_0 decreases with decreasing inter-valley scattering time. Δn_0 vanishes when the inter-valley relaxation time τ' goes to zero.

As has been emphasized, inter-valley scattering is essential to obtain a current induced valley density difference, because it is the channel to exchange electrons between the two valleys. Without inter-valley scattering, the electron density within each valley is exactly conserved.

The valley density difference in Eq. (15) is determined by the first harmonic of the inter-valley scattering rate, which explicitly breaks the discrete rotational symmetry of the system to \mathcal{C}_{1z} . In the next section, we determine the coefficients a_1, a'_1, b_1, b'_1 in Eq. (9) from microscopic modeling of h-BN aligned TBG with \mathcal{C}_{1z} symmetry.

Finally, the valley density difference is proportional to the current, Eq. (15), as we restricted ourselves to linear response. By reversing the current direction, the valley density difference is also reversed, and hence so is the valley polarization, see Eq. (4). Therefore, we conclude that

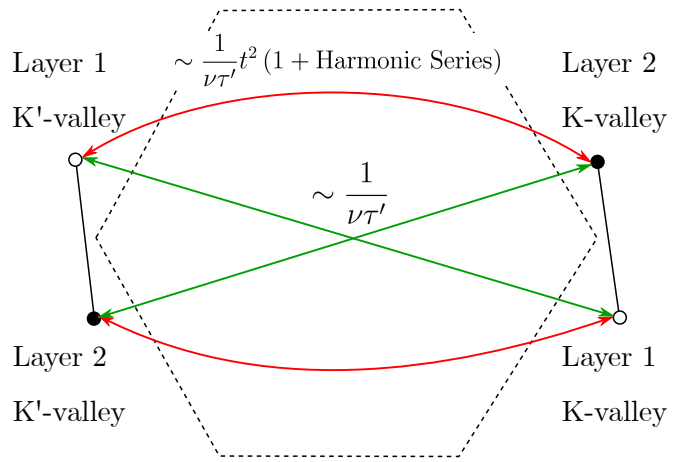


FIG. 6. The inter-valley impurity scattering in twisted bilayer graphene. Layer 1 is strained, while layer 2 is not. The intra-layer inter-valley scattering (green arrows) are assumed to be isotropic. The inter-layer inter-valley scattering (red arrows) may be anisotropic, as in Eq. (9) and Eq. (B14).

with broken rotational symmetry, the valley polarization can be controlled by a DC current.

III.2. Twisted Bilayer Graphene

In this subsection, we estimate the valley density difference for the TBG/h-BN system. As has been emphasized, to induce $\Delta n_0 \neq 0$ from a bias electric field, the lattice rotational symmetry needs to be fully broken. While unaligned TBG exhibits the higher symmetry point group D_3 , a close alignment of either top or bottom TBG layer with h-BN not only breaks the sublattice (inversion) symmetry, but also can induce strain to the sample that further breaks \mathcal{C}_{3z} to \mathcal{C}_{1z} . In the following, we model the rotational symmetry breaking by strain.

A full account of the microscopic details of magic angle TBG to obtain the valley density difference is quite challenging, and requires the full knowledge of the inter-valley scattering mechanism as well as the spectrum and wavefunctions of TBG near the magic twist angle. Nevertheless, the mechanism we proposed in Sec. III.1 is generic. The magnitude of the effect, parametrized by the coefficient δ_ϵ in the valley density difference Eq. (5), is a reflection of the degree of rotational symmetry breaking. For example, in strained single layer graphene, $\delta_\epsilon \sim \epsilon$, where ϵ is the strain strength. In this sense, a general mechanism that enhances the effect of strain would be desirable to explain the small critical current observed in the experiment. In the following, we show that in TBG aligned with h-BN, due to the interplay between two comparable lengths – the moiré scale (a/θ_w) and the strain scale (a/ϵ) – the strain effect is enhanced to $\epsilon \rightarrow \frac{\epsilon}{\theta_w}$. To demonstrate this point, it is enough to introduce the inter-layer tunneling perturbatively, which preserves the analytical solubility.

Our modeling is based on the continuous model, intro-

duced in Ref. 41 and generalized in Ref. 42 that captures elastic deformations systematically. Here, we assume a uniaxial strain parameterized by the strain tensor³⁵

$$\underline{\boldsymbol{\epsilon}} = -\frac{(1+\nu_\epsilon)\epsilon}{2} \begin{bmatrix} \cos 2\phi & \sin 2\phi \\ \sin 2\phi & -\cos 2\phi \end{bmatrix} + \frac{(\nu_\epsilon - 1)\epsilon}{2} \mathbb{I}_2, \quad (16)$$

where ϵ is a dimensionless parameter characterizing the strain strength. $\nu_\epsilon = 0.165$ is the Poisson ratio for graphene. ϕ is the direction of the strain. Note that only the first term in Eq. (16) breaks rotational symmetry and enters into $\boldsymbol{\delta}_\epsilon$.

Without loss of generality, we consider the strain only on layer 1, Fig. 6. Due to the combination of the strain field and the alignment with the h-BN substrate, the Dirac Hamiltonian around the K-point becomes $H = v_D \mathbf{k} \cdot (1 + \boldsymbol{\mathcal{E}}) \cdot \boldsymbol{\sigma} + m\sigma_z$ ⁴², where v_D , \mathbf{k} and m are the Dirac velocity, the momentum measured from the Dirac point and the mass gap, respectively. At the leading order in the strain strength, the rotational symmetry breaking of the continuous model under the strain field is reflected in several aspects. *First*, the Dirac points at $K^{(i)}$ valleys are shifted by $\delta \mathbf{K}_i^{(i)} = -\underline{\boldsymbol{\epsilon}} \cdot \mathbf{K}_i^{(i)}$ for the strained layer⁴². As a result, the momentum difference between the adjacent Dirac points of the two layers, see Fig. 3, is modified as

$$\mathbf{q}_i \rightarrow \mathbf{q}'_i = \mathbf{q}_i - \underline{\boldsymbol{\epsilon}} \cdot \mathbf{K}_i \quad (17)$$

where $\mathbf{q}_i = \theta_w \mathbf{K}_i \times \hat{z}$, $i \in \{1, 2, 3\}$. *Second*, the single layer hopping integral is modified due to the strain field, which modifies the single layer energetics and shift the Dirac points also at order ϵ/a . *Third*, the Dirac spectrum is anisotropic. However, the Dirac spectrum anisotropy is parametrically smaller in $|\mathbf{k}|/|\mathbf{K}|$ than the shift of the Dirac point,⁴² and is thus neglected.

For simplicity, only the first contribution is included in the following discussions. As the wave vectors for inter-layer tunneling $\mathbf{q}'_i - \mathbf{q}'_1$, i.e. the the reciprocal lattice vector of the moiré Brillouin zone (mBZ), are modified due to the strain, the C_3 rotational symmetry of the mBZ is broken explicitly [see Fig. 3(b)], and the effect is characterized by:

$$\frac{\delta \mathbf{K}_\epsilon}{|\mathbf{q}_i|} \sim \frac{\epsilon |\mathbf{K}|}{\theta_w |\mathbf{K}|} = \frac{\epsilon}{\theta_w}, \quad (18)$$

where both the shift of the Dirac point under strain field, $\delta \mathbf{K} \sim \epsilon |\mathbf{K}|$, and the size of mBZ, $q = \theta_w |\mathbf{K}|$, are small and comparable to each other.

We focus on bulk transport. From the discussion of Sec. III.1, both intra- and inter-valley scattering of TBG must be taken into account properly. The dominant scattering mechanism in TBG is yet to be determined, but certain key features may be captured by simple modeling. Here, we consider short range impurities and a low doping level (well below 3/4 filling of the moiré conduction band) so that there is a Fermi pocket around each Dirac point at the corner of the mBZ (see Fig. 6). Notice that the inter-valley scattering involves a much larger momentum transfer than the intra-valley one. Therefore, we assume the intra-valley scattering time τ being much

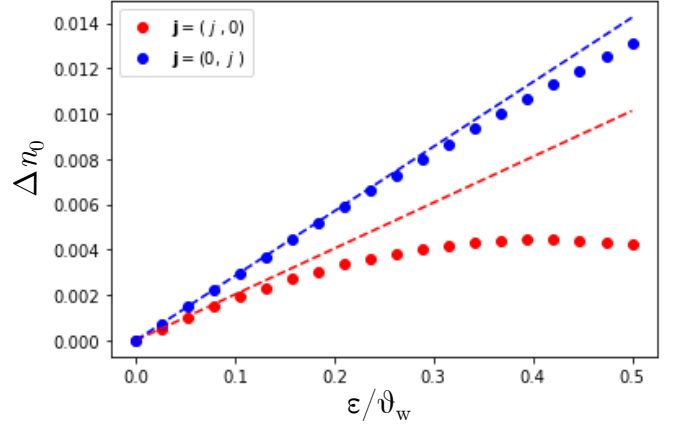


FIG. 7. The valley density difference generated by a DC current in TBG with a strain field. The density is normalized to $\frac{3t^2/4}{1+3t^2/4} \frac{1}{\hbar v_F} \frac{\hbar}{e^2} e j$. The dotted lines are obtained from a numerical calculation. The dashed lines correspond to the analytical expression of Eq. (19) for comparison. The parameters are chosen as $\theta_w = 1.03^\circ$, $\phi = 17.20^\circ$, $v_D q/m = 0.1$ and $v_D k_F/m = 0.005$.

shorter than the inter-valley scattering time τ' , which is expected to be generically true for most scattering mechanisms in TBG.

As discussed in the previous subsection, the intra-valley scattering only plays a secondary role in the generation of valley density difference by a bias DC current. Hence, we assume the intra-valley scattering is dominated by the scattering within each Fermi pocket with a constant relaxation time, τ . The inter-valley scattering requires more careful examination to obtain the coefficients a_1, a'_1, b_1, b'_1 in Eq. (9). There are several processes as shown in Fig. 6. With simple on-site disorder, it turns out that the scattering between the two valleys in the same graphene layer does not break C_{3z} and generate non-zero a_1, a'_1, b_1, b'_1 since we neglected the anisotropy of the Dirac spectrum. Thus, the scattering rates between the two valleys of the same graphene layer are taken to be constant, $(\nu\tau')^{-1}$, as indicated by the green arrows in Fig. 6. At the same time, the scattering rates between the two valleys in different layers may break rotational symmetry through the process indicated by the red arrows in Fig. 6. It is directly related to the shift of the Dirac points due to strain as well as the coherent inter-layer tunneling. As in Fig. 6, the scattering rates of such processes are of order $\sim (\nu\tau')^{-1} t^2$, where t is a dimensionless perturbation parameter for the inter-layer tunneling, Eq. (B13).

After fitting the scattering rates into the semi-classical Boltzmann equation introduced in the previous subsection, we obtain the valley density difference generated by a DC current. The main result is summarized in Fig. 7, where, without loss of generality, only one graphene layer is strained (see Appendix B for more details of the calculation).

When the strain strength is zero, C_{3z} is restored and

the valley density difference is identically zero. For non-zero strain strength, the valley density difference appears as expected from the breaking of C_{3z} symmetry. At small strain strength, the valley density difference is linear in the strain strength:

$$\frac{\Delta n_0}{n_j} = 6(1 + \nu_\epsilon) \frac{v_D k_F}{m} \frac{\epsilon}{\theta_w} \sin(2\phi + \theta_j), \quad (19)$$

where the basic scale for current induced density is $n_j = \frac{3t^2/4}{1+3t^2/4} \frac{1}{\hbar v_F} \frac{h}{e^2} e j$. Here θ_j is the angle of the current, ϕ is the angle of uniaxial strain as defined in Eq. (16). The small numerical value in Fig. 7 is a result of the low doping assumption, where $v_D k_F/m$ is a small parameter with k_F being the Fermi momentum. The result is further suppressed by the inter-layer tunneling t^2 , which is assumed to be small to introduce the inter-layer tunneling perturbatively.

Even though our result, Fig. 7 and Eq. (19), was obtained with a set of very specific assumptions (weak inter-layer coupling and low doping level), some implications can be drawn for real samples. In reality, there are several comparable scale: moiré band width, inter-layer coupling and the mass gap^{41,43}. Therefore, the dimensionless parameter t^2 is not small. In addition, the phenomenon of current switching of valley polarization is observed at three quarter filling. Thus, it is reasonable to expect that the small factor of $v_D k_F/m$ in Eq. (19) is lifted and is on the order of $\mathcal{O}(1)$. Therefore, we conclude that the actual valley density difference can be estimated as:

$$\Delta n_0 \propto \frac{\epsilon}{\theta_w} \frac{1}{\hbar v_F} \frac{h}{e^2} e j \quad (20)$$

with a numerical coefficient on the order of $\mathcal{O}(1)$. Based on the arguments above, one may roughly estimate that a small DC current ($\sim 10^{-3}$ A/m) could generate a large valley density difference on the order of 10^{11} m⁻². This is comparable to the effect of magnetic field ($\sim \nu \mu_B B$ and $B \sim 10$ mT with μ_B being the Bohr magneton)¹.

IV. SUMMARY AND DISCUSSION

In this work, we proposed a mechanism for DC current switching of the valley polarization in the dissipative regime. It was obtained by first determining the dynamics of the valley polarization order parameter (VPOP) in an applied electric field near the Curie temperature T_c , using the nonequilibrium Keldysh formalism. This formalism relates the spontaneous value of the VPOP to the one linearly induced by a current without interactions in the paramagnetic phase. In this way, one sees that sweeping the DC current, and thus varying the current generated valley density difference, the VPOP undergoes a first order phase transition. Consequently, the model reproduces a hysteresis curve in the Hall conductance, consistent with the experiments in Refs.^{1,2}. The current generated valley density difference takes the generic form of Eq. (5) and we repeat here

$$\Delta n_0 \simeq \frac{1}{e v_F} \mathbf{j} \cdot \boldsymbol{\delta}_\epsilon. \quad (21)$$

From a solution of the semi-classical Boltzmann equation, we point out that a proper form of inter-valley scattering that breaks the C_{3z} rotational symmetry is necessary to generate non-zero valley density difference by the transport current. This may be due to strain in TBG aligned with h-BN. Our modeling indicates an enhancement of the strain effect by a factor inversely proportional of the twist angle, i.e. $|\boldsymbol{\delta}_\epsilon| \sim \epsilon/\theta_w$. Together with the reduction of Fermi velocity in magic angle TBG, we argue that these two effects significantly reduce the critical current needed to reverse the Hall conductance.

A few theories have been developed in light of the observation of current switching of valley polarization in the TBG/h-BN sample^{1,35}. The picture developed here relies on the finite scattering time τ , and thus does not apply to the quantum anomalous Hall regime observed at temperature well below T_c . It is also a bulk mechanism. The theoretical analysis in Ref. [1], in contrast, describes a finite-size mechanism which applies in the non-dissipative limit $\sigma_{xx} \ll \sigma_{xy}$, based on edge states. In that limit, each edge state can be described in quasi-equilibrium even in the presence of a current, and thereby Ref. 1 obtains a correction to the edge state Free energy of order I^3 , where I is the edge current, which favors the valley polarization associated with a particular direction of the edge current. Another treatment in the non-dissipative regime explicitly models the forces on a domain wall, Ref. 36. In connection to the present work, we note that Ref. 36 introduces violation of valley conservation in a phenomenological manner. At intermediate temperature below T_c , the system has non-zero valley polarization and orbital magnetization and is in the dissipative transport regime. Ref. [35] presents a mechanism for current reversal of the anomalous Hall effect due to magnetoelectric response. The latter work does not distinguish valley polarization and orbital magnetization, which play very different roles in our treatment due to the quasi-conservation of the former. In any case, the result quoted in Ref. [35] becomes negligible close to T_c . Our work instead is relevant near T_c , when the orbital magnetization of the equilibrium system is too small to be greatly affected by a small critical DC current.

V. ACKNOWLEDGEMENT

We thank Kohei Kawabata for helpful discussions. This research is funded in part by the Gordon and Betty Moore Foundation through Grant GBMF8690 to UCSB to support the work of M.Y. L.B. is supported by the NSF CMMT program under Grant No. DMR-1818533. X.Y. is supported by the Heising-Simons Foundation, the Simons Foundation, and NSF Grant No. NSF PHY-1748958 and partly by NSF Grant No. DMR-1608238 and DMR-2037654.

- ¹ M. Serlin, C. Tschirhart, H. Polshyn, Y. Zhang, J. Zhu, K. Watanabe, T. Taniguchi, L. Balents, and A. Young, *Science* **367**, 900 (2020).
- ² A. L. Sharpe, E. J. Fox, A. W. Barnard, J. Finney, K. Watanabe, T. Taniguchi, M. Kastner, and D. Goldhaber-Gordon, *Science* **365**, 605 (2019).
- ³ E. C. Stoner, *Proceedings of the Royal Society of London. Series A. Mathematical and Physical Sciences* **165**, 372 (1938).
- ⁴ S. L. Sondhi, A. Karlhede, S. A. Kivelson, and E. H. Rezayi, *Phys. Rev. B* **47**, 16419 (1993).
- ⁵ A. H. MacDonald, H. A. Fertig, and L. Brey, *Phys. Rev. Lett.* **76**, 2153 (1996).
- ⁶ Y. Cao, V. Fatemi, A. Demir, S. Fang, S. L. Tomarken, J. Y. Luo, J. D. Sanchez-Yamagishi, K. Watanabe, T. Taniguchi, E. Kaxiras, *et al.*, *Nature* **556**, 80 (2018).
- ⁷ Y. Cao, V. Fatemi, S. Fang, K. Watanabe, T. Taniguchi, E. Kaxiras, and P. Jarillo-Herrero, *Nature* **556**, 43 (2018).
- ⁸ J. F. Dodaro, S. A. Kivelson, Y. Schattner, X. Q. Sun, and C. Wang, *Phys. Rev. B* **98**, 075154 (2018).
- ⁹ L. Zou, H. C. Po, A. Vishwanath, and T. Senthil, *Phys. Rev. B* **98**, 085435 (2018).
- ¹⁰ Y.-H. Zhang, D. Mao, Y. Cao, P. Jarillo-Herrero, and T. Senthil, *Phys. Rev. B* **99**, 075127 (2019).
- ¹¹ L. Balents, C. R. Dean, D. K. Efetov, and A. F. Young, *Nature Physics* , 1 (2020).
- ¹² H. C. Po, H. Watanabe, and A. Vishwanath, *Phys. Rev. Lett.* **121**, 126402 (2018).
- ¹³ Y.-H. Zhang, D. Mao, and T. Senthil, *Phys. Rev. Research* **1**, 033126 (2019).
- ¹⁴ H. Isobe, N. F. Q. Yuan, and L. Fu, *Phys. Rev. X* **8**, 041041 (2018).
- ¹⁵ R. Nandkishore, L. Levitov, and A. Chubukov, *Nature Physics* **8**, 158 (2012).
- ¹⁶ D. V. Chichinadze, L. Classen, and A. V. Chubukov, *Phys. Rev. B* **101**, 224513 (2020).
- ¹⁷ D. V. Chichinadze, L. Classen, and A. V. Chubukov, *Phys. Rev. B* **102**, 125120 (2020).
- ¹⁸ C. Xu and L. Balents, *Phys. Rev. Lett.* **121**, 087001 (2018).
- ¹⁹ H. C. Po, L. Zou, A. Vishwanath, and T. Senthil, *Phys. Rev. X* **8**, 031089 (2018).
- ²⁰ M. Yankowitz, S. Chen, H. Polshyn, Y. Zhang, K. Watanabe, T. Taniguchi, D. Graf, A. F. Young, and C. R. Dean, *Science* **363**, 1059 (2019).
- ²¹ X. Lu, P. Stepanov, W. Yang, M. Xie, M. A. Aamir, I. Das, C. Urgell, K. Watanabe, T. Taniguchi, G. Zhang, A. Bachtold, A. H. MacDonald, and D. K. Efetov, *Nature* **574**, 653 (2019).
- ²² Y. Cao, D. Rodan-Legrain, J. M. Park, F. Noah Yuan, K. Watanabe, T. Taniguchi, R. M. Fernandes, L. Fu, and P. Jarillo-Herrero, *arXiv e-prints* , arXiv:2004.04148 (2020), arXiv:2004.04148 [cond-mat.mes-hall].
- ²³ Y. Jiang, X. Lai, K. Watanabe, T. Taniguchi, K. Haule, J. Mao, and E. Y. Andrei, *Nature* **573**, 91 (2019).
- ²⁴ K. Hejazi, C. Liu, H. Shapourian, X. Chen, and L. Balents, *Phys. Rev. B* **99**, 035111 (2019).
- ²⁵ K. Hejazi, C. Liu, and L. Balents, *Phys. Rev. B* **100**, 035115 (2019).
- ²⁶ Y. Saito, J. Ge, K. Watanabe, T. Taniguchi, and A. F. Young, *Nature Physics* **16**, 926 (2020).
- ²⁷ Y. Xie, B. Lian, B. Jäck, X. Liu, C.-L. Chiu, K. Watanabe, T. Taniguchi, B. A. Bernevig, and A. Yazdani, *Nature* **572**, 101 (2019).
- ²⁸ C. L. Tschirhart, M. Serlin, H. Polshyn, A. Shragai, Z. Xia, J. Zhu, Y. Zhang, K. Watanabe, T. Taniguchi, M. E. Huber, and A. F. Young, *arXiv e-prints* , arXiv:2006.08053 (2020), arXiv:2006.08053 [cond-mat.mes-hall].
- ²⁹ J. Kang and O. Vafek, *Phys. Rev. Lett.* **122**, 246401 (2019).
- ³⁰ H. Polshyn, J. Zhu, M. A. Kumar, Y. Zhang, F. Yang, C. L. Tschirhart, M. Serlin, K. Watanabe, T. Taniguchi, A. H. MacDonald, and A. F. Young, *Nature* **588**, 66 (2020).
- ³¹ N. Bultinck, S. Chatterjee, and M. P. Zaletel, *Phys. Rev. Lett.* **124**, 166601 (2020).
- ³² M. Ochi, M. Koshino, and K. Kuroki, *Phys. Rev. B* **98**, 081102 (2018).
- ³³ M.-C. Chang and Q. Niu, *Journal of Physics: Condensed Matter* **20**, 193202 (2008).
- ³⁴ D. Xiao, M.-C. Chang, and Q. Niu, *Rev. Mod. Phys.* **82**, 1959 (2010).
- ³⁵ W.-Y. He, D. Goldhaber-Gordon, and K. T. Law, *Nature Comm.* **11**, 1 (2020).
- ³⁶ C. Huang, N. Wei, and A. MacDoanld, *arXiv e-prints* , arXiv:2007.05990 (2020), arXiv:2007.05990 [cond-mat.mes-hall].
- ³⁷ A. Kamenev, *Field theory of non-equilibrium systems* (Cambridge University Press, 2011).
- ³⁸ A. Altland and B. D. Simons, *Condensed matter field theory* (Cambridge university press, 2010).
- ³⁹ N. D. Mermin, *Journal of Mathematical Physics* **8**, 1061 (1967).
- ⁴⁰ E. Lifshitz and L. P. Pitaevskii, *Physical Kinetics, Volume 10 (Course of Theoretical Physics)* (Pergamon Press, New York, 1981).
- ⁴¹ R. Bistritzer and A. H. MacDonald, *Proceedings of the National Academy of Sciences* **108**, 12233 (2011).
- ⁴² L. Balents, *SciPost Phys* **7**, 48 (2019).
- ⁴³ H. Kim, N. Leconte, B. L. Chittari, K. Watanabe, T. Taniguchi, A. H. MacDonald, J. Jung, and S. Jung, *Nano Lett.* **18**, 7732 (2018).

Appendix A: Valley Polarization Order Parameter Dynamics from Keldysh Formalism

This section is for the demonstration of the valley polarization in the twisted bilayer graphene (tBLG) with the presence of an external bias. The ‘slow’ dynamics of the valley polarization order parameter, denoted by $\Phi_{\text{cl}}(\mathbf{x}, t)$ and its Fourier transformation $\Phi_{\text{cl}}(\mathbf{q}, \omega)$, is governed by the following action:

$$\begin{aligned} \mathcal{F}[\Phi_{\text{cl}}, \Phi_{\text{q}}] = & U \int \frac{d\omega}{2\pi} \int \frac{d^2q}{(2\pi)^2} \alpha_2(\mathbf{q}, \omega) \Phi_{\text{q}}(-\mathbf{q}, -\omega) \Phi_{\text{cl}}(\mathbf{q}, \omega) \\ & + U \int_{-\infty}^{\infty} dt \int d^2x [\alpha_1(\mathbf{x}, t) \Phi_{\text{q}}(\mathbf{x}, t) + \alpha_3(\mathbf{x}, t) \Phi_{\text{q}}(\mathbf{x}, t) \Phi_{\text{cl}}^2(\mathbf{x}, t) + \alpha_4(\mathbf{x}, t) \Phi_{\text{q}}(\mathbf{x}, t) \Phi_{\text{cl}}^3(\mathbf{x}, t)] \\ & + \mathcal{O}(\Phi_{\text{q}}^2) \end{aligned} \quad (\text{A1})$$

with the saddle-point time evolution equation given by:

$$0 = \left. \frac{\delta \mathcal{F}[\Phi_{\text{cl}}, \Phi_{\text{q}}]}{\delta \Phi_{\text{q}}} \right|_{\Phi_{\text{q}}=0} \quad (\text{A2})$$

Here, Φ_{q} corresponds to the quantum fluctuations of the valley polarization, in the Keldysh language.

The coefficients of α_i is listed below:

$$\alpha_1(\mathbf{x}, t) = n^{(1)}(\mathbf{x}, t) - n^{(2)}(\mathbf{x}, t) = \Delta n_0(\mathbf{x}, t) \quad (\text{A3})$$

$$\alpha_2(\mathbf{q}, \omega) = U \left(\nu + \frac{\pi^2}{3} \nu'' T^2 + \nu \frac{i\omega}{Dq^2 - i\omega} \right) - 1 \quad (\text{A4})$$

$$\alpha_3(\mathbf{x}, t) = -\frac{1}{8} U^2 \int \frac{d^2k}{(2\pi)^2} \partial_{\epsilon_{\mathbf{k}}}^2 [f^{(1)}(\mathbf{k}) - f^{(2)}(\mathbf{k})] \quad (\text{A5})$$

$$\alpha_4(\mathbf{x}, t) = \frac{1}{48} U^3 \int \frac{d^2k}{(2\pi)^2} \partial_{\epsilon_{\mathbf{k}}}^3 [f^{(1)}(\mathbf{k}) + f^{(2)}(\mathbf{k})] = \frac{1}{24} U^3 \nu'' \quad (\text{A6})$$

Notations:

1. Φ_{cl} corresponds to the VPOP Φ_{v} in the maintext;
2. $n^{(i)}(\mathbf{x}, t)$ is the electron density of valley (i);
3. $\nu = \nu(\epsilon_{\text{F}})$ is the electron density of states at Fermi level ϵ_{F} of a given valley, while ν'' is the second derivative of density of states. The valley polarized state is stable when $\nu'' < 0$.
4. U is the Stoner interaction strength;
5. $D \approx \frac{1}{2} v_{\text{F}}^2 \tau$ is the electron’s diffusion constant;
6. T is the temperature;
7. α_3 will be explained in detail later. It involves the difference of the electron’s distribution function in the two valleys, $f^i(\epsilon, \theta)$. Thus, it is proportional to the bias.

1. Model Hamiltonian

We consider a model of the following Hamiltonian:

$$\hat{H} = \hat{H}_0 + V_{\text{dis}} + \hat{H}_{\text{int}} \quad (\text{A7})$$

The first part of the Hamiltonian is given by:

$$\hat{H}_0 = \begin{bmatrix} H^{(+)}(-i\partial_{\mathbf{x}}) + V_{\text{bias}}(\mathbf{x}) & 0 \\ 0 & H^{(-)}(-i\partial_{\mathbf{x}}) + V_{\text{bias}}(\mathbf{x}) \end{bmatrix} \quad (\text{A8})$$

Electrons live in the two valleys described by $H^{(s)}(-i\partial_{\mathbf{x}})$. The two valleys are presumed to be time reversal (TR) related:

$$\mathcal{T} H^{(+)}(-i\partial_{\mathbf{x}}) \mathcal{T}^{-1} = H^{(-)}(i\partial_{\mathbf{x}}) \quad (\text{A9})$$

The system is subject to a bias electric potential $V_{\text{bias}}(\mathbf{x})$.

The second part is the disorder potential:

$$V_{\text{dis}} = \begin{bmatrix} V_0(\mathbf{x}) & V_1(\mathbf{x}) \\ V_1(\mathbf{x}) & V_0(\mathbf{x}) \end{bmatrix} \quad (\text{A10})$$

The electrons experiences intra-valley impurity scattering potential $V_0(\mathbf{x})$ and the inter-valley impurity scattering potential $V_1(\mathbf{x})$. The impurity potentials follow the following probability distribution:

$$\begin{aligned} P[V_0(\mathbf{x})] &= \text{Exp} \left[-\pi\nu\tau \int d^2x |V_0(\mathbf{x})|^2 \right] \\ P[V_1(\mathbf{x})] &= \text{Exp} \left[-\pi\nu\tau' \int d^2x |V_1(\mathbf{x})|^2 \right] \end{aligned} \quad (\text{A11})$$

and following correlation:

$$\langle V_0(\mathbf{x})V_0(\mathbf{x}') \rangle = \frac{\delta^{(2)}(\mathbf{x} - \mathbf{x}')}{2\pi\nu\tau}; \quad \langle V_1(\mathbf{x})V_1(\mathbf{x}') \rangle = \frac{\delta^{(2)}(\mathbf{x} - \mathbf{x}')}{2\pi\nu\tau'} \quad (\text{A12})$$

where $\langle \dots \rangle$ means disorder average.

The third part of the Hamiltonian gives the Stoner interaction between two valleys:

$$\hat{H}_{\text{int}} = U n^{(+)}(\mathbf{x}, t) n^{(-)}(\mathbf{x}, t) \quad (\text{A13})$$

If the interaction is strong enough to the system may develop valley polarization spontaneously at low temperature.

2. Keldysh Formulation

For nonequilibrium and disordered system, it's convenient to use Keldysh formulation to extract the physical features. The formulation is based on the following path integral:

$$\langle \mathcal{Z} \rangle = \int D\bar{\psi}^{(+)} D\psi^{(+)} D\bar{\psi}^{(-)} D\psi^{(-)} e^{i\mathcal{S}[\bar{\psi}^{(+)}, \psi^{(+)}, \bar{\psi}^{(-)}, \psi^{(-)}]} \quad (\text{A14})$$

with the action given by:

$$\mathcal{S} = \int_{\mathcal{C}} dt \int d^2x \left\{ [\bar{\psi}^{(+)}, \bar{\psi}^{(-)}] \left[i\partial_t - \hat{H}_0 \right] \begin{bmatrix} \psi^{(+)} \\ \psi^{(-)} \end{bmatrix} - U \bar{\psi}^{(+)} \psi^{(+)} \bar{\psi}^{(-)} \psi^{(-)} \right\} \quad (\text{A15})$$

The time contour is defined as $\mathcal{C} = \{-\infty, \infty\} \cup \{\infty, -\infty\}$, going from negative infinity to infinity then back to negative infinity.

The dynamics of the valley polarization order parameter may be obtained by a Hubbard-Strantonovich transformation:

$$\langle \mathcal{Z} \rangle = \left\langle \int D\bar{\psi} D\psi D\Phi e^{i\mathcal{S}[\bar{\psi}, \psi, \Phi]} \right\rangle \quad (\text{A16})$$

with the new action:

$$\mathcal{S}[\bar{\psi}, \psi, h] = \int_{\mathcal{C}} dt \int d^2x \left\{ \bar{\psi} \left[i\partial_t - \hat{H}_0 \right] \psi - \frac{1}{4} U [\bar{\psi}\psi]^2 + \frac{1}{2} U \Phi \bar{\psi} \sigma_z \psi - \frac{1}{4} U \Phi^2 \right\} \quad (\text{A17})$$

Here, the fermionic degrees of freedom is compactly written as $\bar{\psi} = [\bar{\psi}^{(+)}, \bar{\psi}^{(-)}]$ and $\psi = [\psi^{(+)}, \psi^{(-)}]^T$. σ_z is the Pauli matrix in the valley space. The valley polarization order parameter Φ couples to the difference of the electron densities in the two valleys $\bar{\psi}\sigma_z\psi$, and the saddle point solution reads:

$$\Phi = \langle \bar{\psi} \sigma_z \psi \rangle \quad (\text{A18})$$

It's convenient to perform a Keldysh rotation before proceeding further:

$$\bar{\psi}_{1/2} = \frac{1}{\sqrt{2}} (\bar{\psi}_+ \mp \bar{\psi}_-), \quad \psi_{1/2} = \frac{1}{\sqrt{2}} (\psi_+ \pm \psi_-), \quad \Phi_{\text{cl/q}} = \frac{1}{2} (\Phi_+ \pm \Phi_-) \quad (\text{A19})$$

Here, the subindex $+(-)$ indicates the fields on the forward (backward) time domain $\{-\infty, \infty\}$ ($\{\infty, -\infty\}$).

After the Keldysh rotation, the action reads:

$$\mathcal{S} = \int_{-\infty}^{\infty} dt \int d^2x \left\{ \check{\psi} \left[G_0^{-1} - V_{\text{dis}} \gamma^{\text{cl}} + \frac{1}{2} U \Phi_{\alpha} \sigma_z \gamma^{\alpha} \right] \check{\psi} - U \Phi_{\text{cl}} \Phi_{\text{q}} \right\} \quad (\text{A20})$$

Here, we assume the total density $\bar{\psi}\psi$ is fixed, thus neglected the term of $-U [\bar{\psi}\psi]^2$. The meaning of $\Phi_{\alpha}\gamma^{\alpha}$ is explained below.

Some notations: The fermionic fields are two component spinor in Keldysh space, $\check{\psi} = [\bar{\psi}_1, \bar{\psi}_2]$ and $\check{\psi} = [\psi_1, \psi_2]^{\text{T}}$. And each component is also a two component spinor in valley space, $\psi_{1/2} = [\psi_{1/2}^{(+)}, \psi_{1/2}^{(-)}]^{\text{T}}$ and similarly for $\bar{\psi}_{1/2}$. V_{dis} is the disorder potential and is a two by two matrix in the valley space. Meanwhile, γ^{α} with $\alpha = \text{cl}, \text{q}$ are the matrices in the Keldysh space:

$$\gamma^{\text{cl}} = \begin{bmatrix} 1 & 0 \\ 0 & 1 \end{bmatrix}; \quad \gamma^{\text{q}} = \begin{bmatrix} 0 & 1 \\ 1 & 0 \end{bmatrix}. \quad (\text{A21})$$

Then, the fermionic degrees of freedom may be integrated out directly:

$$\langle \mathcal{Z} \rangle = \left\langle \int Dh \exp \left\{ -iU \int_{-\infty}^{\infty} dt \int d^2x \Phi_{\text{cl}} \Phi_{\text{q}} + \text{Tr} \ln \left[G_0^{-1} - V_{\text{dis}} \gamma^{\text{cl}} + \frac{U}{2} \Phi_{\alpha} \sigma_z \gamma^{\alpha} \right] \right\} \right\rangle \quad (\text{A22})$$

where $\text{Tr} \ln[\dots]$ includes summation over space, time, Keldysh and internal valley d.o.f. This is a path integral with an action depends on the order parameter. The goal is to find the effective disorder averaged action $\mathcal{F}[\Phi_{\text{cl}}, \Phi_{\text{q}}] = -i \ln \langle \mathcal{Z} \rangle$ that is linear in Φ_{q} , so that that the semiclassical dynamics of the order parameter is given by:

$$0 = \left. \frac{\delta \mathcal{F}[\Phi_{\text{cl}}, \Phi_{\text{q}}]}{\delta \Phi_{\text{q}}} \right|_{\Phi_{\text{q}}=0} \quad (\text{A23})$$

3. Disorder Averaging Process

The first observation is that $\mathcal{S}[\Phi_{\text{cl}}, \Phi_{\text{q}} = 0] = 0$. A direct implication is that when we do power expansion of the $\text{Tr} \ln[\dots]$ in powers of the order parameter Φ_{α} , each term is at least linear in Φ_{q} . Thus, the expansion goes like follows:

$$\begin{aligned} \text{Tr} \ln \left[G_0^{-1} - V_{\text{dis}} \gamma^{\text{cl}} + \frac{1}{2} U \Phi_{\alpha} \sigma_z \gamma^{\alpha} \right] &= \sum_{n=1}^{\infty} \frac{(-1)^{n-1}}{n} \text{Tr} \left[(G_0^{-1} - V_{\text{dis}} \gamma^{\text{cl}})^{-1} \frac{1}{2} U \Phi_{\alpha} \sigma_z \gamma^{\alpha} \right]^n \\ &= \sum_{n=1}^{\infty} \frac{(-1)^{n-1}}{n} \text{Tr} \left[G_{\text{b}} \frac{1}{2} U \Phi_{\alpha} \sigma_z \gamma^{\alpha} \right]^n \end{aligned} \quad (\text{A24})$$

where for brevity, we define $G_{\text{b}} = (G_0^{-1} - V_{\text{dis}} \gamma^{\text{cl}})^{-1}$. Then, we expand the exponential and then do the disorder average and then re-exponentiate the expression. During this process, we keep our accuracy only to linear order in Φ_{q} .

1. Expand the exponential to linear order in Φ_{q} :

$$\exp \{ \text{Tr} \ln [\dots] \} = 1 + \sum_{n=1}^{\infty} \frac{(-1)^{n-1}}{n} \text{Tr} \left[G_{\text{b}} \frac{1}{2} U \Phi_{\alpha} \sigma_z \gamma^{\alpha} \right]^n + \mathcal{O}(\Phi_{\text{q}}^2), \quad (\text{A25})$$

2. Do the disorder average and keeping terms up to Φ^4 :

$$\begin{aligned} \langle \exp \{ \text{Tr} \ln [\dots] \} \rangle &= 1 + U \langle \text{Tr} \left[G_{\text{b}} \frac{1}{2} \Phi_{\alpha} \sigma_z \gamma^{\alpha} \right] \rangle - \frac{1}{2} U^2 \text{Tr} \langle \left[G_{\text{b}} \frac{1}{2} \Phi_{\alpha} \sigma_z \gamma^{\alpha} \right]^2 \rangle \\ &\quad + \frac{1}{3} U^3 \text{Tr} \langle \left[G_{\text{b}} \frac{1}{2} \Phi_{\alpha} \sigma_z \gamma^{\alpha} \right]^3 \rangle - \frac{1}{4} U^4 \text{Tr} \langle \left[G_{\text{b}} \frac{1}{2} \Phi_{\alpha} \sigma_z \gamma^{\alpha} \right]^4 \rangle + \dots \end{aligned} \quad (\text{A26})$$

3. After re-exponentiate Eq. (A26) and including the non-interacting quadratic in Φ term from Eq. (A22), we find the effective disorder averaged action as

$$\begin{aligned} \mathcal{F} = & -iU \text{Tr}[\Phi_{\text{cl}}\Phi_{\text{q}}] + U \langle \text{Tr} \left[G_{\text{b}} \frac{1}{2} \Phi_{\alpha} \sigma_z \gamma^{\alpha} \right] \rangle - \frac{1}{2} U^2 \text{Tr} \langle \left[G_{\text{b}} \frac{1}{2} \Phi_{\alpha} \sigma_z \gamma^{\alpha} \right]^2 \rangle \\ & + \frac{1}{3} U^3 \text{Tr} \langle \left[G_{\text{b}} \frac{1}{2} \Phi_{\alpha} \sigma_z \gamma^{\alpha} \right]^3 \rangle - \frac{1}{4} U^4 \text{Tr} \langle \left[G_{\text{b}} \frac{1}{2} \Phi_{\alpha} \sigma_z \gamma^{\alpha} \right]^4 \rangle + \dots \end{aligned} \quad (\text{A27})$$

Notice that this process of disorder averaging is quite straightforward here. This is because we aim at the semi-classical dynamics of the order parameter and keep our accuracy only to linear order in Φ_{q} . Thus, different terms do not mix (since each term is already linear in Φ_{q} .)

4. The meaning of each term

1. The linear term vanishes in equilibrium due to time reversal symmetry. A bias electric potential may lead to non-zero value as we show in Sec. 5.
2. The quadratic term contains the polarization operator:

$$\sim -\frac{U^2}{2} \Phi_{\text{q}} \Phi_{\text{cl}} \text{Tr} \langle [G_{\text{b}} \sigma_z \gamma^{\text{cl}} G_{\text{b}} \sigma_z \gamma^{\text{q}}]^2 \rangle = iU^2 \Phi_{\text{q}} \Phi_{\text{cl}} \Pi(q, \omega) \quad (\text{A28})$$

The polarization $\Pi(q, \omega)$ in the static limit contributes to the susceptibility of valley polarization order parameter, and drives a 2nd order phase transition to valley polarized state below T_c .

3. Similar to the linear term, the cubic term vanishes in equilibrium due to time reversal symmetry as well. To analyze the leading order non-equilibrium effect due to bias potential, we keep the linear term only and ignore the cubic term, which is smaller by Φ_{cl}^2 near T_c .
4. The quartic term should be proportional to the second derivative of the electron's density of states as in the usual description of the Stoner instability.

To summarize, the non-equilibrium effect is mainly captured by the linear term. The rest captures the interaction effect to the effective action in equilibrium, which has been studied well in the context of Stoner instability. As a result, in the following perturbative expansion in Φ , V_{bias} is considered only in the linear term. To obtain the coefficients for quadratic and quartic terms, we consider $V_{\text{bias}} = 0$.

5. Linear Term

The linear term we are chasing after only contains the Keldysh Green's function:

$$\langle \text{Tr} \left[G_{\text{b}} \sigma_z \gamma^q \frac{\Phi_{\text{q}}}{2} \right] \rangle = \int_{-\infty}^{\infty} dt \int d^2x \frac{\Phi_{\text{q}}(\mathbf{x}, t)}{2} \text{Tr} [\langle G_{\text{b}}^{\text{K}}(\mathbf{x}, \mathbf{x}; t, t) \rangle \sigma_z] \quad (\text{A29})$$

The equal spacetime Keldysh Green's function is the distribution function up to gradient corrections:

$$\langle G_{\text{b}}^{\text{K}} \rangle(\mathbf{x}, \mathbf{x}; t, t) = \int \frac{d\omega}{2\pi} \int \frac{d^2k}{(2\pi)^2} F(\mathbf{x}, t; \mathbf{k}, \omega) [\langle G_{\text{b}}^{\text{R}} \rangle(\mathbf{x}, t; \mathbf{k}, \omega) - \langle G_{\text{b}}^{\text{A}} \rangle(\mathbf{x}, t; \mathbf{k}, \omega)] \quad (\text{A30})$$

The difference of retarded and advanced Green's function is a delta function $G^{\text{R}} - G^{\text{A}} = -i2\pi\delta(\omega - H_0)$. The integration over the frequency puts F on-mass shell, making a real distribution function. Then, integration over momentum gives $\sim 1 - 2n(\mathbf{x}, t)$, with $n(\mathbf{x}, t)$ being the electron density. Note that F is traced with σ_z . Thus,

$$\boxed{U \langle \text{Tr} \left[G_{\text{b}} \sigma_z \gamma^q \frac{\Phi_{\text{q}}}{2} \right] \rangle = iU \int_{-\infty}^{\infty} dt \int d^2x \Phi_{\text{q}}(\mathbf{x}, t) \left[n^{(1)}(\mathbf{x}, t) - n^{(2)}(\mathbf{x}, t) \right]} \quad (\text{A31})$$

the order parameter Φ_{q} couples to the difference in the electron density of the two valleys.

The valley density difference is defined as $\Delta n_0(\mathbf{x}, t) = n^{(1)}(\mathbf{x}, t) - n^{(2)}(\mathbf{x}, t)$ hereafter. $\Delta n_0(\mathbf{x}, t)$ is induced by the bias field only when proper inter-valley scattering is taken into account. For simplicity, we will ignore the electron interaction to obtain Δn_0 . Formally, the self-consistent kinetic equation for F and thus Δn_0 can be obtained as below.

In Keldysh space, the fermionic Green's function has the following structure:

$$G_b = \begin{bmatrix} G_b^R & G_b^K \\ 0 & G_b^A \end{bmatrix} \quad (\text{A32})$$

The Green's function is a function of two space-time coordinates, $G_b = G_b(\mathbf{x}, \mathbf{x}'; t, t')$. It can be written in terms of Wigner coordinates:

$$G_b(\mathbf{x}, t; \mathbf{k}, \omega) = \int d\Delta t \int d^2\Delta x e^{-i\mathbf{k}\cdot\Delta\mathbf{x} + i\omega\Delta t} G_b(\mathbf{x} + \frac{\Delta\mathbf{x}}{2}, \mathbf{x} - \frac{\Delta\mathbf{x}}{2}; t + \frac{\Delta t}{2}, t - \frac{\Delta t}{2}) \quad (\text{A33})$$

The retarded and advanced Green's functions are given by the standard disorder calculation:

$$G_0^{R/A}(\mathbf{x}, t; \mathbf{k}, \omega) = \frac{1}{\omega - H_0(\mathbf{k}, \mathbf{x}) \pm i\delta} + \text{Gradient Corrections} \quad (\text{A34})$$

The Keldysh Green's function may be parameterized as $G^K = G^R \star F - F \star G^A$ (the Wigner coordinates are not written explicitly). The star operation is defined as:

$$\star = \exp \left\{ \frac{i}{2} \left[\overleftarrow{\partial}_{\mathbf{x}} \cdot \overleftarrow{\partial}_{\mathbf{k}} - \overleftarrow{\partial}_{\mathbf{k}} \cdot \overleftarrow{\partial}_{\mathbf{x}} - \overleftarrow{\partial}_t \cdot \overleftarrow{\partial}_{\omega} + \overleftarrow{\partial}_{\omega} \cdot \overleftarrow{\partial}_t \right] \right\} \quad (\text{A35})$$

F plays the role of density matrix with a two by two structure in valley space, satisfying the following equation:

$$- [\omega - H_0 \star F] = \Sigma^K - (\Sigma^R \star F - F \star \Sigma^A) \quad (\text{A36})$$

This formal equation is essentially the Boltzmann equation in some simple cases (neglecting the entanglement between two valleys). It needs to be solved independently. Within mass shell approximation of F , and considering impurity scattering of the form Eq. (A10), we obtain the semi-classical Boltzmann equation [Eq. (6)] in the main text. While the band carries non-zero Chern number, we have checked that the Berry curvature effect does not contribute to valley polarization in the linear response, so it is ignored to obtain Eq. (6).

6. The quadratic term

For the quadratic term, only the equilibrium contribution needs to be considered for our purpose. The quadratic term from interaction reads:

$$\begin{aligned} & -\frac{1}{2}U^2 \text{Tr} \left\langle \left[G_b \frac{1}{2} \Phi_{\alpha} \sigma_z \gamma^{\alpha} \right]^2 \right\rangle \\ & = -\frac{1}{8}U^2 \sum_{\alpha, \beta} \int_{-\infty}^{\infty} dt_1 dt_2 \int d^2x_1 d^2x_2 \Phi_{\alpha}(\mathbf{x}_2, t_2) \Phi_{\beta}(\mathbf{x}_1, t_1) \text{Tr} \langle G_b(\mathbf{x}_1, \mathbf{x}_2; t_1, t_2) \sigma_z \gamma^{\alpha} G_b(\mathbf{x}_2, \mathbf{x}_1; t_2, t_1) \sigma_z \gamma^{\beta} \rangle \end{aligned} \quad (\text{A37})$$

Some observations:

1. Only the term of the form $\Phi_q \Phi_{cl}$ is relevant. The associate coefficient is $\sim \text{Tr} [G_b \sigma_z \gamma^{cl} G_b \sigma_z \gamma^q] \sim \text{Tr} [G_b^R G_b^K + G_b^K G_b^A]$;
2. Current treatment does not have explicit time dependence in the Hamiltonian. Thus, the Green's functions are functions of time difference;
3. At equilibrium, the Keldysh Green's function is of the following form:

$$\langle G_b^K \rangle(\mathbf{x}_1, \mathbf{x}_2; t_1, t_2) = \int \frac{d\epsilon}{2\pi} e^{-i\epsilon(t_1 - t_2)} F(\epsilon) [\langle G_b^R \rangle(\mathbf{x}_1, \mathbf{x}_2; \epsilon) - \langle G_b^A \rangle(\mathbf{x}_1, \mathbf{x}_2; \epsilon)]; \quad (\text{A38})$$

4. For simplicity, the inter-valley scattering in G_b is ignored. As a result, the Green's functions are diagonal in the valley space. We will argue below that the simplification only modify the result quantitatively.

More careful analysis shows that the quadratic term is:

$$\begin{aligned}
& -\frac{1}{2}U^2 \text{Tr}\langle \left[G_b \frac{1}{2} \Phi_\alpha \sigma_z \gamma^\alpha \right]^2 \rangle \\
& = -\frac{1}{4}U^2 \int_{-\infty}^{\infty} dt_1 dt_2 \int d^2x_1 d^2x_2 \Phi_q(\mathbf{x}_2, t_2) \Phi_{cl}(\mathbf{x}_1, t_1) \\
& \times \text{Tr}\langle G_b^K(\mathbf{x}_1, \mathbf{x}_2; t_1, t_2) \sigma_z G_b^R(\mathbf{x}_2, \mathbf{x}_1; t_2, t_1) \sigma_z + G_b^A(\mathbf{x}_1, \mathbf{x}_2; t_1, t_2) \sigma_z G_b^K(\mathbf{x}_2, \mathbf{x}_1; t_2, t_1) \sigma_z \rangle
\end{aligned} \tag{A39}$$

What's in the trace should be $G^R \sigma_z G^K \sigma_z + G^K \sigma_z G^A \sigma_z$. Since we assumed the Green's functions are diagonal in the valley space, the summation over valley index only contribute to a factor 2.

Next step is to rewrite the fields and Green's functions in frequency space, one arrives at the following expression:

$$\begin{aligned}
& -\frac{U^2}{2} \int \frac{d\omega}{2\pi} \int d^2x_1 d^2x_2 \Phi_q(\mathbf{x}_2, -\omega) \Phi_{cl}(\mathbf{x}_1, \omega) \\
& \times \int \frac{d\epsilon}{2\pi} \langle G_b^K(\mathbf{x}_1, \mathbf{x}_2; \epsilon) G_b^R(\mathbf{x}_2, \mathbf{x}_1; \epsilon + \omega) + G_b^A(\mathbf{x}_1, \mathbf{x}_2; \epsilon) G_b^K(\mathbf{x}_2, \mathbf{x}_1; \epsilon + \omega) \rangle
\end{aligned} \tag{A40}$$

where the valley d.o.f. has been summed over. The second line can be further expressed as

$$\begin{aligned}
& \int \frac{d\epsilon}{2\pi} \left[\langle G_b^R(\mathbf{x}_1, \mathbf{x}_2; \epsilon + \omega) G_b^R(\mathbf{x}_2, \mathbf{x}_1; \epsilon) F(\epsilon + \omega) - G_b^A(\mathbf{x}_1, \mathbf{x}_2; \epsilon + \omega) G_b^A(\mathbf{x}_2, \mathbf{x}_1; \epsilon) F(\epsilon) \right. \\
& \quad \left. + \langle G_b^R(\mathbf{x}_1, \mathbf{x}_2; \epsilon + \omega) G_b^A(\mathbf{x}_2, \mathbf{x}_1; \epsilon) (F(\epsilon) - F(\epsilon + \omega)) \rangle \right] \\
& = -2i \Pi(\mathbf{x}_1, \mathbf{x}_2; \omega)
\end{aligned} \tag{A41}$$

$\Pi(\mathbf{x}_1, \mathbf{x}_2; \omega)$ is the disorder averaged polarization operator, note that the disorder average should be performed for both single particle Green's function and four-point correlation (i.e. the ladder diagrams), and its Fourier component is given by:

$$\Pi(\mathbf{q}, \omega) = \nu + \frac{\pi^2}{3} \nu'' T^2 + \nu \frac{i\omega}{Dq^2 - i\omega}, \quad \text{for } q < l^{-1}, \omega < \tau^{-1} \tag{A42}$$

Thus, in momentum \mathbf{q} and frequency ω space, the quadratic term is given by:

$$\boxed{-\frac{1}{2}U^2 \text{Tr}\langle \left[G_b \sigma_z \gamma^\alpha \frac{\Phi_\alpha}{2} \right]^2 \rangle = iU^2 \int \frac{d\omega}{2\pi} \int \frac{d^2q}{(2\pi)^2} \Phi_q(-\mathbf{q}, -\omega) \Pi(\mathbf{q}, \omega) \Phi_{cl}(\mathbf{q}, \omega)} \tag{A43}$$

In the static limit, i.e. $\omega = 0, \mathbf{q} \rightarrow 0$, we obtain the standard expression for T_c of valley polarization as $1 - U(\nu + \frac{\pi^2}{3} \nu'' T_c^2) = 0 \rightarrow T_c = \sqrt{\frac{U\nu-1}{U\pi^2|\nu''|/3}}$.

7. The cubic and the quartic term

For completeness, we present the calculation for the cubic and the quartic terms.

The cubic term can be very similarly written down:

$$\begin{aligned}
& \frac{1}{3}U^3 \text{Tr}\langle \left[(G_0^{-1} - V_{\text{dis}} \gamma^{cl})^{-1} \frac{1}{2} \Phi_\alpha \sigma_z \gamma^\alpha \right]^3 \rangle \\
& = U^3 \int dt_1 dt_2 dt_3 \int d^2x_1 d^2x_2 d^2x_3 \frac{1}{8} \Phi_q(\mathbf{x}_2, t_2) \Phi_{cl}(\mathbf{x}_3, t_3) \Phi_{cl}(\mathbf{x}_1, t_1) \\
& \times \text{Tr}\langle G(\mathbf{x}_1, \mathbf{x}_2; t_1, t_2) \sigma_z \gamma^q G(\mathbf{x}_2, \mathbf{x}_3; t_2, t_3) G(\mathbf{x}_3, \mathbf{x}_1; t_3, t_1) \rangle
\end{aligned} \tag{A44}$$

Notice that the last line should have been $\sim G \sigma_z \gamma^q G \sigma_z \gamma^{cl} G \sigma_z \gamma^{cl}$, which could be simplified.

The steps to proceed:

1. Put all the Φ fields at the same space-time point (\mathbf{x}_2, t_2) . With this approximation, we neglect the nonlocal effects. We choose the space-time coordinate of Φ_q as a reference point;

2. Expand the Keldysh Green's function as

$$G^K(\mathbf{x}_1, \mathbf{x}_2; t_1, t_2) = \int dt_3 \int d^2x_3 [G^R(\mathbf{x}_1, \mathbf{x}_3; t_1, t_3)F(\mathbf{x}_3, \mathbf{x}_2; t_3, t_2) - F(\mathbf{x}_1, \mathbf{x}_3; t_1, t_3)G^A(\mathbf{x}_3, \mathbf{x}_2; t_3, t_2)] \quad (\text{A45})$$

3. The cubic term would reduce to:

$$\begin{aligned} & \sim \frac{1}{8}U^3 \int dt_2 d^2x_2 \Phi_q(\mathbf{x}_2, t_2) h_{\text{cl}}^2(\mathbf{x}_2, t_2) \int dt_1 dt_3 dt_4 \int d^2x_1 d^2x_3 d^2x_4 \\ & \times \text{Tr} \langle \sigma_z [F(4, 2)G^R(2, 3)G^R(3, 1)G^R(1, 4) - F(2, 4)G^A(4, 3)G^A(3, 1)G^A(1, 2)] \rangle \end{aligned} \quad (\text{A46})$$

Here, (i, j) is short for $(\mathbf{x}_i, \mathbf{x}_j; t_i, t_j)$;

4. The second line may be evaluated in Fourier space, giving rise to $\sim i2\pi \int \frac{d^2k}{(2\pi)^2} \partial_{\epsilon_k}^2 [f^{(1)}(\mathbf{k}) - f^{(2)}(\mathbf{k})]$;

5. The third order term is:

$$\boxed{\sim \frac{-i}{8}U^3 \int dt_2 d^2x_2 \Phi_q(\mathbf{x}_2, t_2) \Phi_{\text{cl}}^2(\mathbf{x}_2, t_2) \int \frac{d^2k}{(2\pi)^2} \partial_{\epsilon_k}^2 [f^{(1)}(\mathbf{k}) - f^{(2)}(\mathbf{k})]} \quad (\text{A47})$$

One should notice that the cubic term vanishes in equilibrium. Thus, it involves the weak electric field and higher order of VPOP. Thus, the cubic term is neglected in the main text, when we discuss the VPOP physics close to or above the critical temperature, T_c .

The quartic term can be evaluated in the same way as the cubic term:

$$\begin{aligned} & -\frac{1}{4}U^4 \text{Tr} \langle [G_b \frac{1}{2} \Phi_\alpha \sigma_z \gamma^\alpha]^4 \rangle \\ & = -U^4 \int dt_1 dt_2 dt_3 dt_4 \int d^2x_1 d^2x_2 d^2x_3 d^2x_4 \frac{1}{16} \Phi_q(\mathbf{x}_2, t_2) \Phi_{\text{cl}}(\mathbf{x}_3, t_3) \Phi_{\text{cl}}(\mathbf{x}_4, t_4) \Phi_{\text{cl}}(\mathbf{x}_1, t_1) \\ & \times \text{Tr} \langle G(\mathbf{x}_1, \mathbf{x}_2; t_1, t_2) \gamma^q G(\mathbf{x}_2, \mathbf{x}_3; t_2, t_3) G(\mathbf{x}_3, \mathbf{x}_4; t_3, t_4) G(\mathbf{x}_4, \mathbf{x}_1; t_4, t_1) \rangle \end{aligned} \quad (\text{A48})$$

The next steps fully parallel the previous analysis of the cubic term:

1. Put all the Φ fields at the same space-time point (\mathbf{x}_2, t_2) . With this approximation, we neglect the nonlocal effects, which does not alter our main conclusion. We choose the space-time coordinate of Φ_q as a reference point;
2. Expand the Keldysh Green's function as, e.g.

$$G^K(\mathbf{x}_1, \mathbf{x}_2; t_1, t_2) = \int dt_3 \int d^2x_3 [G^R(\mathbf{x}_1, \mathbf{x}_3; t_1, t_3)F(\mathbf{x}_3, \mathbf{x}_2; t_3, t_2) - F(\mathbf{x}_1, \mathbf{x}_3; t_1, t_3)G^A(\mathbf{x}_3, \mathbf{x}_2; t_3, t_2)]; \quad (\text{A49})$$

3. The quartic term would reduce to:

$$\begin{aligned} & \sim -\frac{1}{8}U^4 \int dt_2 d^2x_2 \Phi_q(\mathbf{x}_2, t_2) \Phi_{\text{cl}}^3(\mathbf{x}_2, t_2) \int dt_1 dt_3 dt_4 dt_5 \int d^2x_1 d^2x_3 d^2x_4 d^2x_5 \\ & \times \langle [F(5, 2)G^R(2, 3)G^R(3, 4)G^R(4, 1)G^R(1, 5) - F(2, 5)G^A(5, 3)G^A(3, 4)G^A(4, 1)G^A(1, 2)] \rangle \end{aligned} \quad (\text{A50})$$

Here, (i, j) is short for $(\mathbf{x}_i, \mathbf{x}_j; t_i, t_j)$;

4. The second line may be evaluated in Fourier space, giving rise to $\sim \frac{i}{3!} \int \frac{d^2k}{(2\pi)^2} \partial_{\epsilon_k}^3 [f^{(1)}(\mathbf{k}) + f^{(2)}(\mathbf{k})]$;

5. The fourth order term would be:

$$\boxed{\begin{aligned} & \sim -\frac{i}{48}U^4 \int dt d^2x \Phi_q(\mathbf{x}, t) \Phi_{\text{cl}}^3(\mathbf{x}, t) \int \frac{d^2k}{(2\pi)^2} \partial_{\epsilon_k}^3 [f^{(1)}(\mathbf{k}) + f^{(2)}(\mathbf{k})] \\ & = i\frac{1}{24}U^4 \nu'' \int dt d^2x \Phi_q(\mathbf{x}, t) \Phi_{\text{cl}}^3(\mathbf{x}, t) \end{aligned}} \quad (\text{A51})$$

8. Equation of Motion

Combining the calculation above, one can obtain the action given at the beginning of this section. The equation of motion for the valley polarization order parameter Φ_{cl} could also be read out as:

$$\Delta n_0 + [U\Pi(q, \omega) - 1] \Phi_{\text{cl}} + \alpha_3 \Phi_{\text{cl}}^2 + \frac{1}{24} U^3 \nu'' \Phi_{\text{cl}}^3 = 0 \quad (\text{A52})$$

Appendix B: Modeling of Twisted Bilayer Graphene (TBG)

This section presents the necessary technical details of our modeling of the twisted bilayer graphene. Our modeling is based on BM's continuous model in Ref.⁴¹ and its generalization to the situation with an arbitrary smooth lattice deformation in Ref.⁴².

1. The Model Hamiltonian for TBG under uniaxial strain

As an example, we focus on the electronic states near the K-point of layer 1, which can be well described by the following Hamiltonian:

$$H^{(1K)}(\mathbf{k}) = \begin{bmatrix} h_{-\theta_w/2}^{(+)}(\mathbf{k}) & T_b & T_{tr} & T_{tl} \\ T_b^\dagger & h_{\theta_w/2}^{(+)}(\mathbf{k} + \mathbf{q}'_b) & 0 & 0 \\ T_{tr}^\dagger & 0 & h_{\theta_w/2}^{(+)}(\mathbf{k} + \mathbf{q}'_{tr}) & 0 \\ T_{tl}^\dagger & 0 & 0 & h_{\theta_w/2}^{(+)}(\mathbf{k} + \mathbf{q}'_{tl}) \end{bmatrix} \quad (\text{B1})$$

where θ_w is the twist angle. As argued in the maintext, we are neglecting the anisotropy in the Dirac Hamiltonian. Therefore, the diagonal terms are given by:

$$h_{\theta}^{(+)}(\mathbf{k}) = \begin{bmatrix} m & v_{\text{D}} k e^{-i(\theta_{\mathbf{k}} - \theta)} \\ v_{\text{D}} k e^{-i(\theta_{\mathbf{k}} - \theta)} & -m \end{bmatrix} \quad (\text{B2})$$

where $k = |\mathbf{k}|$ and $\theta_{\mathbf{k}} = \tan^{-1} \frac{k_y}{k_x}$ are the magnitude and the polar angle of momentum \mathbf{k} measured from the K-point, respectively; the diagonal element, m , is the mass term induced by the alignment with the substrate.

The inter-layer coupling are described by the off-diagonal terms in Eq. (B1), given by^{41,42}:

$$T_b = w \begin{bmatrix} 1 & 1 \\ 1 & 1 \end{bmatrix}, \quad T_{tr} = w e^{-i\mathbf{g}'(2) \cdot \mathbf{d} + i\mathbf{g}(2) \cdot \boldsymbol{\tau}} \begin{bmatrix} 1 & e^{i\frac{2\pi}{3}} \\ e^{-i\frac{2\pi}{3}} & 1 \end{bmatrix}, \quad T_{tl} = w e^{-i\mathbf{g}'(3) \cdot \mathbf{d} + i\mathbf{g}(3) \cdot \boldsymbol{\tau}} \begin{bmatrix} 1 & e^{-i\frac{4\pi}{3}} \\ e^{i\frac{4\pi}{3}} & 1 \end{bmatrix}, \quad (\text{B3})$$

where w is the inter-layer coupling strength; $\mathbf{g}^{(i)}(2, 3)$ are the reciprocal lattice vector of the graphene layer 1(2); \mathbf{d} and $\boldsymbol{\tau}$ are vectors defining the twist in real space: $\mathbf{R}' = M(\theta_w)(\mathbf{R} - \boldsymbol{\tau}) + \mathbf{d}$. Here, the effect of any strain field is also neglected. The strain field will introduce corrections in the reciprocal lattice vectors. Thus, the corrections to the inter-layer couplings are on the order of strain strength.

More importantly are the momenta \mathbf{q}'_i with $i = 1, 2, 3$ (or b, tr, tl), which connect the K-point in layer 1 to the adjacent K-point in layer 2, Fig. 3(b). Mathematically, the momenta \mathbf{q}'_i are given by:

$$\mathbf{q}'_i = \mathbf{q}_i - \boldsymbol{\mathcal{E}} \cdot \mathbf{K}_i; \quad \mathbf{q}_i = |\mathbf{K}| \theta_w \times \left\{ (0, -1), \left(\frac{\sqrt{3}}{2}, \frac{1}{2} \right), \left(-\frac{\sqrt{3}}{2}, \frac{1}{2} \right) \right\} \quad (\text{B4})$$

where $\boldsymbol{\mathcal{E}}$ is the uniaxial strain tensor; \mathbf{K}_i are the momenta of the three K-points of layer 1. Here, we consider only layer 1 is strained, without loss of generality.

For the convenience of analytical calculation, one may assume the inter-layer coupling is weak and solve for the wavefunction perturbatively for the states around the K-point, $|\mathbf{k}| \ll |\mathbf{q}_i|$. The wavefunction will be used to evaluate the impurity scattering amplitudes and the rates.

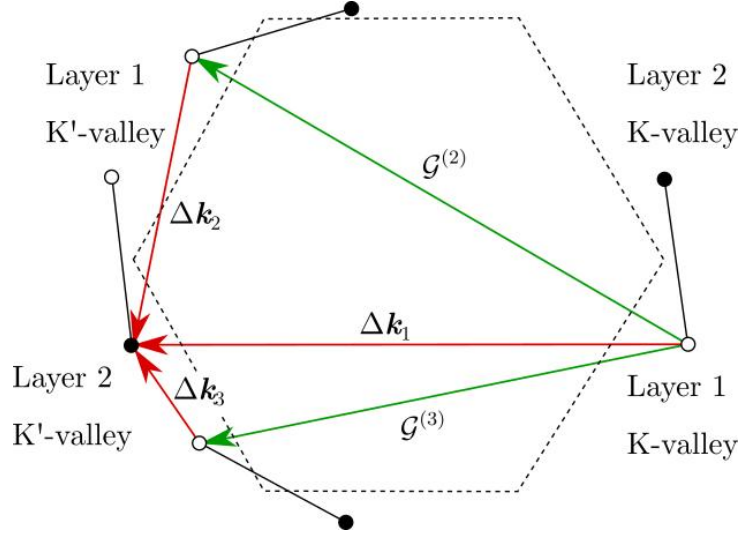


FIG. 8. The possible momentum transfers $\Delta\mathbf{k}_i$ (red) upon impurity scattering between states of K-valley layer 1 and K' valley layer 2. The green arrows labels the reciprocal lattice vectors $\mathcal{G}^{(2,3)}$ of graphene layer 1.

2. Impurity Potential and Impurity Average

In this section, we present the details about the impurity potential and impurity averaging process in our simplified model calculation. For the convenience of analytical calculation, we assumed short ranged impurities (for simplicity), whose functional form in real space is given by:

$$V(\mathbf{r}) = V\delta(\mathbf{r} - \mathbf{R}_{\text{imp}}). \quad (\text{B5})$$

Therefore, for a scattering process of plane waves with momentum transfer of $\Delta\mathbf{k}$, the scattering amplitude is given by the Fourier transformation:

$$V(\Delta\mathbf{k}) = Ve^{i\Delta\mathbf{k}\cdot\mathbf{R}_{\text{imp}}} \quad (\text{B6})$$

Here the phase factor is kept explicitly. It will be important below when doing the disorder averaging in the huge moiré unit cell.

Let's focus on the scattering between the two valleys of different layers, indicated by the red arrows in Fig. 6. We start the analysis by assuming only the sublattice A of graphene layer 2 is disordered and evaluating the scattering rates. Then, one should do the same analysis for the disorder to be on the other sublattice site and the other graphene layer and do an algebraic average over the all the scattering rates.

Let's focus on the situation when only the sublattice A of graphene layer 2 is disordered. The scattering amplitude from a state \mathbf{k} near the K-point of layer 1 to a state \mathbf{k}' near the K'-point of layer 2 is given by:

$$V_{\mathbf{k}'\mathbf{k}}^{(2K')(1K)} = \psi_{\mathbf{k}'}^{(2K')\dagger} \hat{V}^{(2A)} \psi_{\mathbf{k}}^{(1K)} \quad (\text{B7})$$

where $\psi_{\mathbf{k}}^{(1K)}$ and $\psi_{\mathbf{k}'}^{(2K')}$ are the wavefunctions of the states near K-point of layer 1 and K'-point of layer 2 correspondingly. The impurity matrix is given by an 8-by-8 matrix:

$$\hat{V}^{(2A)} = V \left[\begin{array}{c|cc|cc|cc} 0_{2\times 2} & e^{i\Delta\mathbf{k}_1\cdot\mathbf{R}_{\text{imp}}} & 0 & e^{i\Delta\mathbf{k}_2\cdot\mathbf{R}_{\text{imp}}} & 0 & e^{i\Delta\mathbf{k}_3\cdot\mathbf{R}_{\text{imp}}} & 0 \\ & 0 & 0 & 0 & 0 & 0 & 0 \\ \hline 0_{6\times 2} & & & 0_{6\times 6} & & & \end{array} \right] \quad (\text{B8})$$

The corresponding scattering rate is defined as:

$$W_{\mathbf{k}'\mathbf{k}}^{(2K')(1K)} = 2\pi\rho_{\text{imp}} \left| V_{\mathbf{k}'\mathbf{k}}^{(2K')(1K)} \right|^2 \quad (\text{B9})$$

where ρ_{imp} is the impurity density.

Notice that the moiré lattice has a huge unit cell. Therefore, Eq. (B9) is not yet the scattering rate to be put in the Boltzmann equation. The scattering rate to be used in the Boltzmann equation is obtained from Eq. (B9) by

averaging over the impurity location \mathbf{R}_{imp} . The disorder averaging can be easily done by noticing that the phases in the impurity matrix, Eq. (B8), are completely random relative to each other. Algebraic, this can be seen by factoring out the factor $e^{i\Delta\mathbf{k}_1 \cdot \mathbf{R}_{\text{imp}}}$ in Eq. (B8). The remaining phases involve the momentum difference. Notice that

$$\Delta\mathbf{k}_2 - \Delta\mathbf{k}_1 = \mathcal{G}(2), \quad \Delta\mathbf{k}_3 - \Delta\mathbf{k}_1 = \mathcal{G}(3) \quad (\text{B10})$$

where $\mathcal{G}(2/3)$ are the reciprocal lattice constant of graphene layer 1. Notice that the impurities are now assumed to be in graphene layer 2. The relative phases can be written as:

$$\begin{aligned} e^{i(\Delta\mathbf{k}_{2/3} - \Delta\mathbf{k}_1) \cdot \mathbf{R}_{\text{imp}}} &= e^{i\mathcal{G}(2/3) \cdot \mathbf{R}_{\text{imp}}} = e^{i[\mathcal{G}(2/3) - \mathcal{G}'(2/3)] \cdot \mathbf{R}_{\text{imp}}} \\ &= e^{i\mathcal{G}^M(2/3) \cdot \mathbf{R}_{\text{imp}}}. \end{aligned} \quad (\text{B11})$$

In the last equally of the first line, the reciprocal lattice vector of graphene layer 2, $\mathcal{G}'(2/3)$ is inserted. To go to the second line, one should notice that the difference of the reciprocal lattice vector of the two graphene layers defines the the reciprocal lattice vector of the moiré lattice, $\mathcal{G}^M(2/3)$. At this point, due to the huge moiré unit cell, it's obvious that the relative phases in Eq. (B8) are completely random upon impurity averaging. The disorder averaging of the scattering rates can be done by averaging the random phases:

$$\langle W_{\mathbf{k}'\mathbf{k}}^{(2K')(1K)} \rangle_{\text{imp}} = 2\pi\rho_{\text{imp}} \langle |V_{\mathbf{k}'\mathbf{k}}^{(2K')(1K)}|^2 \rangle_{\text{imp}} \quad (\text{B12})$$

with \mathbf{R}_{imp} being the location of the impurities, whose values correspond to the locations of the sublattice A of graphene layer 2. Algebraically, this disorder averaging process is the same as independently treating each nonzero element in Eq. (B8) and calculating the scattering rates and then doing an averaging.

3. Scattering Rates

Following the procedure in the previous subsection, we were able to calculate the impurity scattering rate and extract the valley density difference under a DC current with numerical calculation. The result is summarized as the dotted line in Fig. (7).

Under certain limit, analytical expressions can be found to help understand the limiting factors of the valley density difference under a DC current. Below, we present the scattering rates under the limit of $v_D |\mathbf{k}^{(\prime)}| = v_D k_F \ll v_D |\mathbf{q}_i| \ll m$ and $\epsilon \ll \theta_w$ as well as the weak inter-layer coupling limit. The first condition, $v_D k_F \ll v_D |\mathbf{q}_i| \ll m$, states that the chemical potential is close to the bottom (top) of the conduction (valence) band so that the Fermi surfaces are approximately circular. The second condition, $\epsilon \ll \theta_w$, assumes weak strain strength so that the the rotational symmetry is weakly broken. The last simplification of weak inter-layer coupling manifests itself as the condition of:

$$t = \frac{w}{v_D^2 \mathbf{q}_i^2 / 2m} \ll 1. \quad (\text{B13})$$

Under the conditions stated above, we were able to find the leading order contribution to the inter-valley, inter-layer scattering rates (indicated as red arrows in Fig. (6)) for electrons in the conduction band:

$$\begin{aligned} W_{\mathbf{k}'\mathbf{k}}^{(2K')(1K)} &\approx \frac{1}{\nu\tau'} \frac{3}{4} t^2 \left\{ 1 + \left[3(\epsilon_{xx} - \epsilon_{yy}) \frac{\epsilon}{\theta_w} \frac{k_F}{q} - 3\epsilon_{xy} \frac{\epsilon}{\theta_w} \frac{v_D k_F}{m} \right] \cos \theta_{\mathbf{k}} + \left[-6\epsilon_{xy} \frac{\epsilon}{\theta_w} \frac{k_F}{q} - \frac{3}{2} (\epsilon_{xx} - \epsilon_{yy}) \frac{\epsilon}{\theta_w} \frac{v_D k_F}{m} \right] \sin \theta_{\mathbf{k}} \right. \\ &\quad \left. + \left[-3(\epsilon_{xx} - \epsilon_{yy}) \frac{\epsilon}{\theta_w} \frac{k_F}{q} - 3\epsilon_{xy} \frac{\epsilon}{\theta_w} \frac{v_D k_F}{m} \right] \cos \theta_{\mathbf{k}'} + \left[6\epsilon_{xy} \frac{\epsilon}{\theta_w} \frac{k_F}{q} - \frac{3}{2} (\epsilon_{xx} - \epsilon_{yy}) \frac{\epsilon}{\theta_w} \frac{v_D k_F}{m} \right] \sin \theta_{\mathbf{k}'} \right\} \end{aligned} \quad (\text{B14})$$